A PRELIMINARY STUDY TOWARDS MM-WAVE WIRELESS NETWORK TOPOLOGY OPTIMIZATION USING RAY TRACING

MASTER THESIS REPORT

A PRELIMINARY STUDY TOWARDS MM-WAVE WIRELESS NETWORK TOPOLOGY OPTIMIZATION USING RAY TRACING

MASTER THESIS REPORT

Thesis

to obtain the degree of Master of Science
in Electrical Engineering
at Delft University of Technology
to be defended publicly on
29 August 2022 at 13:00 o'clock

by

Xiangwen WANG

born in Hubei, China

This dissertation has been approved by
Promotor: Prof. DSc. A. Yarovoy

Thesis committee:

Prof. DSc. A. Yarovoy,	Delft University of Technology, *Professor, Chairman*
Dr. Remco Litjens,	Delft University of Technology, *Associate Professor*
Dr. Y. Aslan,	Delft University of Technology, *Assistant Professor*

CONTENTS

ACKNOWLEDGEMENTS

Time flies so fast that my two years of study at TU Delft draws to an end, and it feels like just yesterday that I commenced this adventure, leaving my family and friends behind to come to the Netherlands. I am fortunate and appreciative to choose TUD for my master's studies and to have the opportunity to learn and grow. I have gained much invaluable knowledge and cherished memories during this study time, which are my enduring treasures.

First and foremost, I would like to express my great gratitude to my daily supervisor, Dr. Y. Aslan. Throughout my entire thesis project, he provides me with continuous guidance, enthusiastic support, inspiring suggestions, and great patience. Even when our meetings exceeded the scheduled time, he continued to patiently address my questions until we figure the problem out. And I am deeply appreciative of his detailed comments and feedback on my thesis report even at 4 a.m.

I would also like to express my gratitude to my supervisor, Prof. DSc. A. Yarovoy. I really appreciated his help with the opportunity of the internship at Siemens and the opportunity of a thesis project. His insightful advice for my thesis project, presentation skills, thesis report writing, and English language skills for reading and writing gave me many helpful guidance.

I am also thankful to MSc W. Bouwmeester, who offered assistance when I faced challenges in downloading and using WinProp. And I am grateful for discussions with peer students with many great inspirations. The entire MS3 team, including professors, PhDs, and support staff, has created a supportive, warm, and perfect environment, and I am grateful to be within this wonderful atmosphere where I have completed my master's thesis.

Lastly, I would like to thank my parents and friends for their continuous warm emotional support during challenging moments.

In the future, what I have learned here will definitely help me to overcome many challenges. And I hope happiness always finds its way to those who have helped me in this journey.

ABSTRACT

Increasing wireless communication requirements of data rates, capacity and coverage, and evolution and maturation of wireless equipment prompt wireless communication research insight concentrating on millimeter wave (mm-wave) frequency. However, high reflection coefficients and high path loss cause large shadow areas (e.g. behind the buildings) and poor coverage, leading to constraints on wireless connectivity and effectiveness of wireless communication. Intelligent Reflecting Surface (IRS) is a revolutionizing technology in 6th-generation mobile networks (6G), which achieves extended coverage with reducing construction and electricity costs via its characteristics of passive beamforming and proper deployment, and auxiliary of Ray Tracing (RT) facilitates obtention and analysis of channel state information (CSI) at different locations. With the objective of developing a flexible RT tool and a novel methodology for optimal IRS deployment to maximize coverage in non-line-of-sight (NLOS) areas from the BS, a new RT simulation model is built in this thesis project in accordance with measured data, leading to improved reliability and accuracy of 5.3% maximum error in path loss. And a novel, but preliminary, weight graph methodology is proposed for tackling the IRS deployment problem for coverage extension in NLOS areas quasi-optimally. To integrate the IRS with RT simulation, a first-time comparison between metal reflectors and IRS under realistic EM effects is exploited. The obtained simulation results unveil that deploying IRS with the proposed weight graph methodology facilitates wireless coverage improvement, and the coverage probability increased from 0% to 96.23% with a threshold of -75 dBm under 28 GHz in a selected Region of Interest (RoI).

keywords - mm-wave Wireless communication, Intelligent reflected surface, ray tracing, electromagnetics propagation, optimization, urban areas, weight graph

ABBREVIATIONS

5G 5th-generation mobile networks. 1

6G 6th-generation mobile networks. ix

AF Amplify-and-Forward. 12

BS Base Station. 2

CDF Cumulative Distribution Function. 10

CSI Channel State Information. ix

DF Decode-and-Forward. 12

EE Energy Efficiency. 12

EM Electromagnetic. 14

FD Full-Duplex. 13

HPPPs Homogeneous Poisson Point Processes. 13

IAB Integrated access and backhaul. 11

IRS Intelligent Reflecting Surface. ix

IRT intelligent Ray Tracing. 19

LGCP Log-Gaussian Cox Process. 10

LOS Line-of-Sight. 2

MIMO Multiple-Input Multiple-Output. 1

mm-wave millimeter wave. ix

NLOS Non-Line-of-Sight. ix

NN Neural Networks. 13

OSM OpenStreetMap. 14

PPP Poisson Point Process. 10

QoS Quality of Service. 10

RF Radio Frequency. 2

RMS Root-Mean-Square. 8

RoI Region of Interest. ix

RT Ray Tracing. ix

SNR Signal-to-Noise Ratio. 12

TU/e Technische Universiteit Eindhoven. 4

1

INTRODUCTION

This chapter presents an introduction to this thesis work. Section 1.1 provides an overview of the background of mm-wave wireless communication, IRS, and RT, as well as the motivation behind this work. Section 1.2 presents the research questions about the deployment of passive IRS in a hybrid wireless network, and the goals to achieve. Then Section 1.3 lists the research scope and assumptions in this work. Section 1.4 and Section 1.5 detail the novelties and contribution of this work, as well as the structure of the thesis.

1.1. MOTIVATION

To achieve high data rates and large bandwidth, electromagnetic waves in the mm-wave frequency range spanning from 30 GHz to 300 GHz are exploited in the 5th-generation mobile networks (5G) currently, and will be utilized in the 6G in the future. Besides extreme capacity and abundant available spectrum that other frequencies can not deliver, small antenna size, higher resolution, and limited propagation range associated with low interference are also the advantage offered by the millimeter wave [1]. However, these characteristics also present challenges, such as different propagation mechanisms (high penetration losses [2], high reflection coefficients [2], reduced diffraction, high path loss) from the waves at traditionally used sub-6 GHz bands, which result in large shadow areas and poor coverage [3], thereby constraining wireless connectivity and limiting the effectiveness of other mm-wave applications. In 5G communication, massive multiple-input multiple-output (MIMO) has been used to tackle the problem, which however has the crucial issues of high hardware complexity, increased computing power demands, and expensive implementation and deployment costs [4]. As one of the key and revolutionizing technology for 6G networks, IRS will play a similar crucial role in 6G networks to massive MIMO in 5G networks [5].

IRS is a planar surface consisting of massive low-cost unit cells, which makes it feasible to passively beamforming and reflect electromagnetic waves. The way of beamforming control divides the IRS into reconfigurable IRS and non-reconfigurable IRS, in which the former one controls the state of PIN diode or the values of resistors

in each reflecting element [6–8] for software-controllable amplitude and phase, and the latter one modifies the design and composition construction to realize passively beamforming, and this research considers the non-reconfigurable (fixed) IRS. Compared to active relay and massive MIMO systems, IRS operates passively in a full-duplex mode without any active transmit module or energy-consuming hardware, such as the radio frequency (RF) chains. On account of which this innovative technology facilitates mounting on different surfaces at a low cost, with high energy efficiency and simpler interference management for ubiquitous wireless connectivity [7–10].

The proper passive IRS deployment in the IRS-aided wireless network (Fig 1.1) is imperative for achieving extended coverage, optimizing propagation channels, reducing deployment cost, and minimizing electricity consumption [11, 12], and it can also simplify the precoding design at the base stations (BS) [13]. **The objective of this thesis work are (i) to develop a reliable (w.r.t. measured data) simulation tool for coverage assessment, and (ii) to use the tool with a novel, yet preliminary, methodology to integrate IRS and optimize their deployment (angles and positions).** Deploying nodes judiciously requires exhaustive CSI, which can be challenging to analyze in different real-world scenarios. RT can be performed to obtain CSI at all locations, enabling analysis of large-scale fading characteristics (e.g., path loss, shadow fading) [14], temporal characteristics (e.g., delay spread) [15, 16], and received power distribution [17] in urban environments with mm-wave frequencies. Since deploying IRS to balance line-of-sight (LOS) and NLOS links and to extend coverage in a wireless network in a complex urban scenario with high accordance to the reality still remains a challenge deserving of tackling [18], **this thesis approaches to the IRS-aided mm-wave network coverage enhancement problem by making use of RT to plot received power levels with the novel idea of correlating the metal reflector electromagnetic performance to the IRS.**

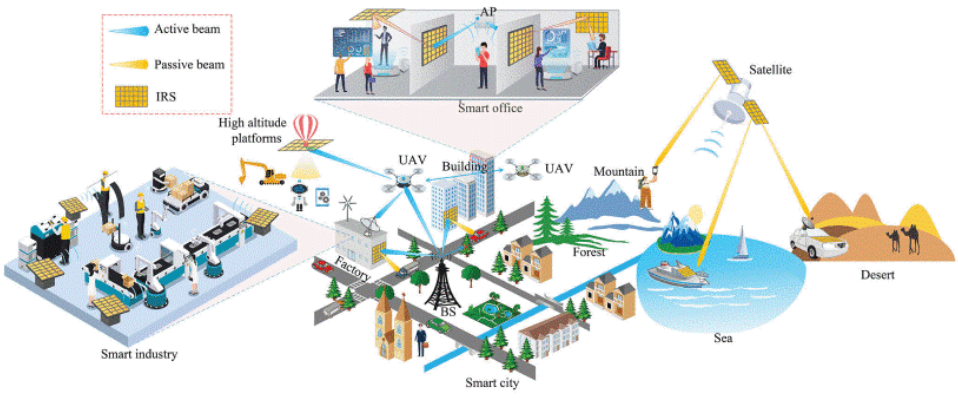

Figure 1.1: IRS application deployment scenarios [19]

1.2. RESEARCH PROBLEM AND GOALS

The deployment of IRS is an indispensable step in constructing a 6G IRS-aided network and integrating IRS into the future network. However, there are several recognized research challenges and problems related to IRS deployment that deserve further investigation or careful consideration. This section outlines the recognized problems as follows:

1. IRS is a new technology, and there is scarce literature about the practical deployment of IRS in a complex environment. And most of the existing works about the deployment in IRS-aided networks are with given IRS and BS locations or under random or intuitively selected locations. Therefore, researches about deploying IRS in simulated complicated scenario still needs more investigation and maybe lack reference, which can be one of the problems. (see Subsection 2.3.2 for the relevant literature)

2. IRS simulation is not supported in existing software. To fulfill the requirement of reflector deployment using RT, how to characterize the IRS in the RT simulation is a challenge. (see Subsection 2.3.3 for the relevant literature)

3. RT is a good method to obtain CSI precisely and directly. However, the simulation of ray propagation is based on the scenario information, like the building layout, which means for the first step of RT model simulation, accurate site information is of vital significance (see Subsection 2.3.3 for the relevant literature). Another problem for RT is the characteristic of site specificity, which may constrain the autonomous deployment for IRS. [8] Tuning the RT scenario to have a good match to the real scenario is essential.

4. With the development of 4G and 5G wireless networks, there have been multiple deployment topologies for ubiquitous active devices practically, like BSs or relays (see Subsection 2.2.2 for the relevant literature). However, there are differences between the deployment of IRS and BS in the traditional wireless network, on account of which the IRS deployment can not directly refer to the optimal active device deployment schemes that have been researched. For example, without signal amplifying circuits and transmit RF chains, the IRS operating ranges are usually much shorter than the range of BS [8].

5. Because of the high reflection coefficients and high penetration losses of mm-waves, the NLOS paths are much weaker than LOS path [20]. To achieve high spatial multiplexing, placing a sufficiently large number of IRS in the NLOS area away from BS and receiver are critical, which is a trade-off between the path loss and spatial multiplexing [8].

Considering all the research problems above, the ultimate goal of this project is to develop a flexible RT tool and a novel methodology for optimal IRS deployment to maximize coverage in NLOS areas from the BS. And the research tasks are formulated as follows:

1. Creating a RT computational model in Altair HyperWorks WinProp with similar settings and environments as a related published model.
2. Performing RT simulations for the urban scenario and comparing the area coverage with evaluation metrics in the RT model with them in the published scenarios.
3. Developing a novel methodology and obtaining the optimal positions of IRSs in the simulated scenarios.
4. Verification of the results by comparing the coverage with no reflector installment and arbitrarily selected reflector installment in the same simulated scenarios.

1.3. RESEARCH SCOPE AND ASSUMPTIONS

In this thesis project, the research scope and assumptions are listed as follows:

- One simulation environment is considered in this thesis project, which is based on one part in the Technische Universiteit Eindhoven (TU/e) campus [21].
- A fixed BS position with a fixed antenna beam is utilized and simulated in the RT simulation model.
- The inter-cell or intra-cell interference is not considered in this project, and the work is based on coverage evaluation. And one single NLOS area is selected for analysis as a proof-of-concept.
- There is 1D control in beamforming for the non-reconfigurable IRS in this thesis project. And this project only considers azimuthal beamforming.
- A passive IRS in comparison with the metal plate is assumed. And reconfigurable IRS may bring additional losses because of the different structures and components to the non-reconfigurable IRS that is used in this work.
- Vertical polarization is utilized in RT simulation. (see Section 4.1 for more generic assumptions in RT)

1.4. THESIS NOVELTIES AND CONTRIBUTION

With the objective of signal coverage improvement by optimizing the IRS parameters utilizing RT and the abovementioned problems, the main contributions and novelties of this research are listed as follows:

1. **A new RT simulation setup with improved reliability based on measured data.** To improve the consistency of the RT simulated scenario with reality, the simulated scenario construction in this research is substantiated with real ground truth, which is the real measured data from Dr. Robbert Schulpen's Ph.D. thesis report from TU/e [21].

2. **First-time comparison of metal reflectors with IRS under realistic EM effects.** Exploiting the two reflectors' realistic EM effects and deployment of metal reflector deployment facilitates the determination of optimal IRS's position and angle.

3. **First-time consideration of practical factors of IRS** (incidence-reflection angle, dependent losses, polarization effect) in RT simulated scenario **with existing RT software** combined with CST IRS simulation.

4. **A novel methodology by constructing a weighted graph in improving coverage in NLOS areas by optimal reflection direction and distribution of IRS** is proposed in this research.

1.5. THESIS STRUCTURE

The rest of the report is organized as follows. Chapter 2 introduces the current research related to RT, deployment of BS and IRS, and listed the IRS-related works utilizing RT. Chapter 3 provides the research framework and simulation workflow in the simulator first, then describes the simulated model including the scenario, BS, and reflector simulation. Parameter settings in RT processing and the model validation compared with ground truth are demonstrated in Chapter 4. The model optimization is detailed in Chapter 5, aiming at reflector deployment optimization. Simulation results and analysis are then shown in Chapter 6 to assess the influence of reflector, weight accuracy, and the optimal IRS position in example situations. Finally, conclusions and recommendations are summarized in Chapter 7.

2

Background and Literature Review

This chapter discusses the related works regards to RT, deployment of BS, and IRS. Section 2.1 explains the principle of the RT method, and illustrates the studies with RT in indoor or outdoor environments, and related commercial simulators. Section 2.2 introduces the network deployment background first and presents related studies in BS deployment with 5G technology and RT. The introduction of IRS and its applications, studies about IRS deployment, and utilization of RT in IRS-related research are indicated in Section 2.3.

2.1. Ray Tracing (RT)

2.1.1. RT Principle

RT is a method to depict and analyze all the possible ray paths propagation from transmitter to receiver, which is a good tool to assist in designing wireless systems. The RT simulation phases include ray generation, ray intersection, and rendering [22]. For mm-wave propagation with high penetration attenuation, the general interactions are reflection, diffraction, and transmission, which can be described by image-RT approach and ray launching algorithm generally in RT.

For the image-RT approach [23], a visibility tree (Fig 2.1) is constructed recursively in the algorithm, consisting of the tree root corresponding to the transmitter, the first layer containing the objects in the LOS area from the transmitter, and the n^{th} layers corresponding to the objects in the LOS area from the $(n-1)^{th}$ layers. Then each ray is cast from objects in the former layer to corresponding objects in the latter layer. The ray launching algorithm [16, 23] produces rays discretely by meshing a wave sphere into many equilateral triangles in the spherical reference system, and each ray is represented by each line launching from the spherical center to each triangle. Also, there will be a sphere around the receiver, the receiver receives the rays that intersect with the sphere. The field strength will be calculated in the propagation. The ray launching algorithm is less computationally complex than the image-RT

approach, but the inherent discretization may lead to blind area [23]. Since the passive beamforming of IRS is also discrete with massive reflecting elements [8], RT can be a good method to simulate the wave propagation and interaction with exploiting IRS.

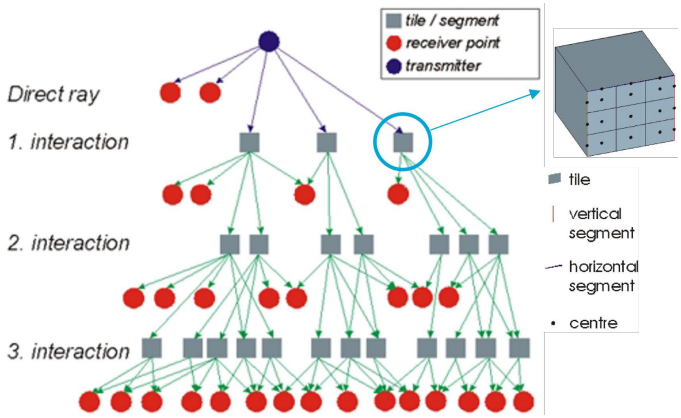

Figure 2.1: Image-RT approach [24]

2.1.2. RT-RELATED STUDIES

RT is applied to optical propagation problems first at the beginning of the nineties [23, 25]. From then on, the application of RT in mm-wave wireless network systems achieves increasingly widespread attention. Under indoor environments, B. Ai et al. [26] investigated the massive MIMO channel performance using their own developed RT simulator, and concluded that in the same indoor scenario, the measurement and the RT-based simulation results reached a good agreement, with evaluating path loss, shadow fading, root-mean-square (RMS) delay spread, and coherence bandwidth. Besides B. Ai et al., the good consistency between the measured results and RT simulated results is confirmed in the research of M. Gao et al. [27] and S. Li et al. [28]. Furthermore, B. Neekzad et al. [29] and S. Kishimoto et al. [30] revealed the prediction ability of RT for cluster locations, ray arrival statistics within clusters, and measured channels in the indoor environment, which shows the possibility and high effectiveness in analyzing indoor millimeter wave channel with RT.

In the application of RT under outdoor environments, Guan-yun Wang et al. [16] and M. Dong et al. [31] presented initial fundamental studies on coverage and BS deployment in simple urban street canyon scenarios, which provides the foundation for future deployment research. For the sake of analyzing channel characteristics more practically, there are studies exploiting RT based on real-city scenarios, such as building distributions in Ottawa [17], Chengdu [14], and Seoul [15]. Besides with buildings, Vitucci, E. M. et al. [32] tuned a RT model to analyze and predict mm-wave urban propagation based on a real scenario with scattering objects such as

trees and vehicles, and found the effect of scattering from nonspecular components in the RT prediction accuracy, which is important for RF coverage in outdoor urban scenarios.

With gathered momentum in utilizing RT, there are some available commercially RT-based simulators, such as Wireless Insite and WinProp (Fig 2.2), that can be used for mm-wave coverage prediction, wireless network planning, and BS deployment [33]. Y. Zhou et al. [34] used Wireless Insite to establish and simulate an indoor mm-wave propagation model, based on which they proposed the relation between large-scale path loss, angle spread and carrier frequencies, and antenna positions. Y. Aslan et al. [35] used WinProp to analyze the performance of single-lobe beam and multi-lobe beam antenna arrays in urban outdoor environments.

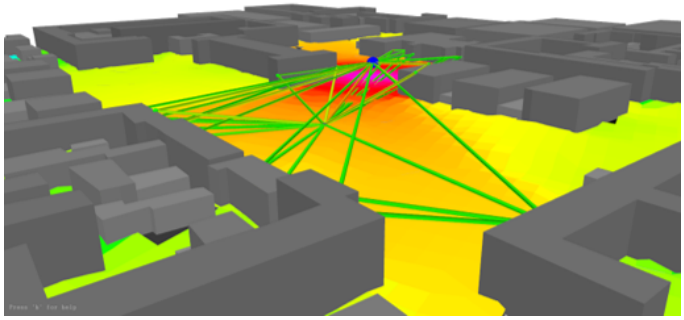

Figure 2.2: 3D ray tracing in an urban scenario in Feko WinProp

In conclusion, RT is feasible to simulate and analyze wave propagation and interaction in mm-wave urban environments, and there have been open RT simulators, among which WinProp is the simulator utilized in this project.

2.2. BASE STATION(BS) DEPLOYMENT

2.2.1. BS DEPLOYMENT BACKGROUND

A BS is a fixed transceiver that is the infrastructure to connect mobile devices in wireless communication systems. With the significant momentum of wireless communication from 2G to 5G networks, the installation of BSs is witnessed a rapidly increasing demand all over the world for ubiquitous wireless connectivity [36]. Taking into account energy consumption, cost, signal coverage, and signal quality, the optimal spatial distribution model of BSs is indispensable and of vital significance.

In the 1940s, Bell Laboratories proposed the cellular concept, and V. H. M. Donald introduces the principle of cellular system operating for the large-scale mobile-telephone service [37]. In the cellular concept, the hexagonal layout was the

ideal way to segregate a service area into cells, which achieves a larger coverage with the minimum number of transmitters. The relative positions of transmitters to the hexagon depend on the direction of the antennas, for example, the omnidirectional antenna can be deployed in the center of a hexagon, while the directional antenna can be deployed at the corner of a hexagon.

One of the most popular models [38] in the cellular network is setting the BSs at the corner to form a hexagon, which facilitates frequency reuse but can not be adopted in current deployments with heterogeneous BSs. And the tractable Poisson Point Process (PPP) model [38, 39] has been adopted frequently for network deployment in single-operator networks, but since the operators' clustering and environmental obstacles result in the density difference in the BS deployment, there are some gaps when deploying BS with multiple operators. J. Kibiłda et al. [39] studied the BS deployment stochastic geometry models based on real deployment data from three European countries, and with the coverage probability as the evaluation metric, they concluded that the coverage using the log-Gaussian Cox process (LGCP) model with stable correlation function is the closest to the real multi-operator network. L. Chiaraviglio et al. [38] studied the BS distributions in urban, rural, and coastal zones based on real data sets obtained from Italy and Croatia, and concluded that the BS probability density in urban scenarios fits the α-Stable distribution most.

2.2.2. BS DEPLOYMENT IN 5G

The BS deployment in the 5G cellular network is different from its predecessors, because of its relatively poor penetration ability, smaller coverage area, and higher deployment cost. C. -H. Wang et al. [40] studied the trade-off between signal coverage and installation cost to establish 5G macro and micro BSs. In their research, for the microcell which is used in a densely populated urban area, they used a clustering algorithm for the initial BS location, and then proposed a mixed-integer nonlinear optimization scheme to achieve minimum cost and maximum coverage. And the authors in [41] introduced a meta-heuristic algorithm based on swarm intelligence for optimal deployment. However, in practical BS deployment, the obstacle will also have a significant influence on wave propagation, which is investigated in [42]. The authors proposed a scenario sampling approach and analyzed the BS urban street deployment problem into an integer linear problem (ILP). After utilizing the iterative algorithm and evaluating with Pathloss distribution and cumulative distribution function (CDF) of the violation probability, they solved the optimization problem with low complexity.

Besides deployment topology in the theoretical and mathematical aspects, there are researches tackling the deployment problem combined with more realistic urban construction. Ensuring the satisfaction of the Quality of Service (QoS) and cost reduction, Q. Zeng [43] proposed a method to establish BSs in an optimal deployment strategy under a given map, which is about applying the Canny Edge

Detection, Opening Operation algorithms, and Quadtree Traversal Algorithm to form the graph based on the given map and decide the deployment points.

Additionally, utilizing RT in the BS deployment is feasible, and has been implemented in some research. H. Miao and L. Xiong [44] exploited RT in the design of 5G network in an urban rail traffic station, and estimated the system by path loss, RMS delay spread, Ricean K-factor, angular spread, etc. Furthermore, based on RT, P. Tang [45] investigated 5G in an urban rail station with path loss, etc. as well, and summarized some BS deployment suggestions in the Rail Station. In [46], the authors proposed Integrated access and backhaul (IAB) deployments for a massive coverage with a small number of fiber-connected BSs, and demonstrated with RT. With Altair WinProp, C. Bektas et al. [47] proposed an unsupervised learning-based and clustering-based network planning framework for suitable antenna placement solutions, and evaluated the results with coverage ratio and power distribution as the heat maps in RT simulation.

From the above literature, BS deployment study development has been relatively mature. However, active BS deployment topologies are different from passive IRS, indicating that IRS deployment can not directly refer to the optimal active device deployment schemes [8], and the scale of the simulated scenario in this project limits the BS deployment so that only one BS will be used in this project without considering multiple BS deployment topology. And some coverage performance metrics (e.g. CDF) are worthy of reference.

2.3. INTELLIGENT REFLECTING SURFACE(IRS) AND ITS DEPLOYMENT

2.3.1. IRS INTRODUCTION

IRS is a planar surface with massive reflected elements integrated on it, which could achieve amplitude and phase control, and 3D passive beamforming for cooperative signal focusing and interference cancellation [8, 12].

For reconfigurable IRS, there are typically three layers [8], which are unit cells printed on a dielectric substrate, a copper plate, and a control circuit board. Each mata-atom represents an equivalent circuit consisting of a PIN diode and/or a variable resistor load [48], [49], and by switching the state of the PIN diode or tuning the value of the resister, the phase and the amplitude of the reflected signal could be coordinately controlled in π in rad and in [0, 1] respectively. The second layer with copper is used to avoid signal energy leakage, while the inner layer can connect and be controlled by a field-programmable gate array (FPGA) to adjust the state of each reflected element.

Different designs of structures for non-reconfigurable IRS are proposed for controllable amplitude and phase. [50], [51], and [52] proposed different IRS designs with patch antenna type backscatter tag, cross loop and square ring slot, and

orthogonal groups of parallel dipoles separately. By modifying the unit cell electrical size, loop length, and dipole length respectively, reflection phase variation is feasible in these non-reconfigurable IRSs, which leads to controllable passive beamforming.

With great potential and advantages, there are mainly four IRS research directions in the literature, which are hardware impairments, channel estimation [53–55], passive beamforming design [56], and IRS deployment [8, 19, 57]. Among these for the direction of IRS deployment, by deploying the IRS nodes judiciously and controlling the passive beamforming, the typical applications can be eliminating the dead zone [12], creating signal hotspots at the cell edge [58], improving the throughput by increasing the transmission path [56], and increasing indoor signal coverage extension [57]. This project concentrates on coverage improvement, which is introduced specifically in Subsection 2.3.2.

2.3.2. IRS-Assisted Wireless Networks Deployment

As one of the research directions, deployment of IRS with BS is critical and indispensable for practically exploiting IRS in the advent of the wireless communication revolution.

Before researching how to deploy IRS massively, the studies on the IRS start with whether the IRS is an innovative technology with actual value, by comparing it with active devices. Since one of the main use for IRS is the extension of BS signal coverage and beamforming the received signal to the destination, the half-duplex relays have the same usage as IRS [59], which has been utilized in reality. In [60], C. Huang et al. compared IRS with an ideal amplify-and-forward (AF) relay in a simple scenario with one BS, one obstacle, one IRS/relay, and K users. Neglecting the direct path between the BS and the users, and evaluating by Energy Efficiency (EE) and system Spectral Efficiency in bps/Hz, the authors proposed that there are up to 300% higher EE can be provided in the IRS-aided system than applying AF relay. However, since decode-and-forward (DF) relay works better than AF relay in achievable rates, E. Björnson et al. [59] compared IRS with DF relay in the consideration of both LOS and NLOS path. By evaluating the transmit power needed to achieve a given rate and EE, they observed that to be competitive, IRS requires hundreds of reflected elements to compensate for the low channel gain. But because of the sub-wavelength size of each element, the IRS with hundreds of elements will be physically rather small.

To investigate whether IRS-system could be utilized to fulfill the requirement of BS signal coverage extension, under the most simple scenario with one BS, one IRS, and one user, Q. Wu et al. [8, 61] compared the BS minimum transmit power required for achieving user signal-to-noise ratio (SNR) of 20 dB, and demonstrated that IRS could create a “signal hotspot” in its vicinity. On account of which to achieve given SNR at receivers, IRS could save transmit power at the BS, which also means effective BS signal coverage extension. Furthermore, the authors also compared the normalized interference power and minimum transmit power in the scenario with multiuser, the

results make it substantiated that with IRS, the interference power and the required transmit power in their algorithm are significantly reduced.

For a more complicated scenario with single-IRS or double-IRS, B. Zheng et al. [62] and Y. Han et al. [63] studied the multi-user effective channel rank, maximum SNR and average received SNR in the single-IRS system and the double-IRS cooperative system with a given sufficient total number of IRS elements, and observed that the performance with two cooperative IRS is substantially better than that with one IRS. The comparison results validate the feasibility of massive IRS deployment.

For the environment with more IRSs, J. Lyu et al. in [56, 64] investigated the performance of the system of multiple IRSs randomly deployed in the cell. In [64], the author set a BS in the center of a cell and uniformly deployed the users randomly, and compared the deployment range with an increasing number of randomly deployed relays and IRSs. The results showed that there is an optimal number of IRSs for the deployment range, and with the increasing number of IRS or full-duplex (FD) relays, the spatial throughput with IRS can be superior to that with FD relays. In [56], the authors set multiple BS, multiple IRSs, and one user randomly by independent homogeneous Poisson point processes (HPPPs), and concluded that increasing IRS installment density and the increasing number of IRS reflecting elements could facilitate the increasing coverage probability. When the IRS installment density is large enough, more elements could result in growing IRS passive beamforming gain and larger coverage. Moreover, by evaluating spatial throughput, they observed that there is an optimal IRS/BS density ratio. However, they did not consider the obstacles, which are indispensable in practical deployment. In [65], M. A. Kishk et al. modeled the BSs locations as a PPP, the blockages as a line boolean model, and got IRS locations by deriving the indirect path probability from a given user-BS link, and found that IRSs deployment could improve the BSs coverage regions in the scenario with blockages.

Besides stochastic geometry, it is also feasible to tackle the deployment problem with Neural Networks (NN). In [66], C. Liaskos et al. investigated the indoor scenario with one transmitter, one receiver, and walls installed with IRS. By configuring the input layer with the number of transmitters and receivers, densities and dimensions of IRS, and other propagation environment parameters, the authors proposed a NN approach and obtained the optimal IRS signal interaction point and propagation channel for achieving maximum received power.

As introduced above, in most available studies, the IRS deployment topologies are simple, and to the best of my knowledge, the first attempt to simulate and analyze the IRS deployment in a large-scale typical urban environment (e.g. Hangzhou in China) with buildings and vegetation in the 5G network is [67]. B. Sihlbo et al. simulated the environment with Coffee Grinder Simulator which has no available open access now, and used the already deployed 5G network and IRS simulation model in it. With equipping uniformly random users and an already deployed 5G network, the simulator uses an iterative method to obtain the optimal deployment

of IRSs by calculating the SNR for the cell-edge users. After deploying IRS and comparing it with the scenario without IRS, the authors demonstrated that the coverage probability and per block rate will increase significantly.

However, from the most related literature [67], for the IRS deployment algorithm, they utilized an iterative algorithm to simulate all the 3D RT models with different IRS deployment possibilities, which is time-consuming and inefficient. For the simulation scenario model, they integrated their system with OpenStreetMap (OSM) API directly, providing the top-view shape and maximum height of buildings, and partial tree positions with the same size, which means that they lost some information about irregular shape buildings, all the tree position and their different sizes, grass, and ground. For the IRS simulation, they considered 0 dB reflection Losses for each IRS. However, practical IRS reflection loss is related to incident wave angle and desired reflected wave angle [52]. Consideration of algorithm efficiency, scenario model, and IRS simulation consistency with reality is indispensable.

2.3.3. IRS WITH RT

It is substantiated to exploit RT in the research of IRS. For the IRS research direction of channel estimation, D. Dampahalage et al. [68] used Remcom Wireless InSite to simulate the RT scenario, and evaluate their two IRS channel estimation reduction schemes. D. Ding et al. [69] proposed a scheme for beam selection effectively and quantified the results with RT in Remcom Wireless InSite. As for the IRS research direction of beamforming, utilizing RT in Winprop, Y. Xing et al. [57] presented the optimal phase shift of IRSs.

Table 2.1: Details on RT in the IRS-related literature

Ref	Goal	IRS simulation	f/GHz	RT tool	Scenario
[68]	Channel estimation reduction	A planar reflecting array of 16×16 reflecting elements	24.2	Remcom Wireless InSite	outdoor
[69]	Beam selection	100 × 100 reflecting elements with a DFT based passive beamforming codebook	\	Remcom Wireless InSite	outdoor
[57]	Optimal phase shift for IRS beamforming	16 × 16 reflecting elements	28	Winprop	indoor outdoor
[66]	Optimal interaction point NN performance evaluation	Tile with Electromagnetic (EM) functions (steer, collimate, absorber) installed on the wall	2.4	PWE simulator	indoor
[67]	IRS deployment in large -scale urban environment	Anomalous reflector with different size (0.33m*0.33m, etc.)	28	Coffee Grinder Simulator (not open)	outdoor
[70]	A new ray tracing simulator proposal	8 × 8 passive elements	2.3	WiThRay (not open)	outdoor

For IRS deployment with RT, in [66] which is introduced before about using NN to determine the optimal interaction point, the authors simulated with RT and compared the received powers in different channel methods to evaluate their NN performance. Furthermore, in [67], the simulator realizes propagation simulation

and power distribution with RT. In [70], a new simulator is proposed for RT and is exploited to model the IRS response based on electromagnetics.

More details of utilizing RT in the IRS-related literature are shown in Table 2.1. From the literature, there are scarce studies about exploiting RT in the research of IRS, and even fewer in IRS deployment at 28 GHz. No existing open software support IRS simulation, so with existing software, the authors simulate IRS with small sizes consisting of a small amount of reflecting elements, which does not show good agreements with practical IRS and would affect IRS performance [59]. Additionally, except [67], all the simulated scenario models in the above literature are very simple, with several building blocks or several walls, on account of which, a new RT simulation model with improved reliability is of vital significance.

2.4. CONCLUSION

In this chapter, the literature for research on RT, BS deployment, and IRS are discussed. For RT, the principle of it, RT-related studies under indoor or outdoor environments, and under real-city scenarios, and the two commercially RT-based simulators are introduced. For the BS deployment, the cellular concept and popular models in the cellular network are demonstrated first, and BS deployment based on theoretical, mathematical, and RT are discussed separately. Finally, for the IRS-related literature, the constitution of the IRS plate, IRS deployments, and related works about RT simulation with IRS are demonstrated in detail, which illustrates the feasibility and executability of exploiting RT in the IRS network deployment.

Based on the above review of the existing literature, the gaps and limitations of the field are summarized as follows:

- There has been multiple relatively mature research on BS deployment topology, some of which even take practical implementation into account. However, due to the complexity of integrating the IRS with RT and assessing the electromagnetic performance of the IRS-assisted networks, optimal IRS deployment in a given NLOS environment is more challenging than BS deployment topologies presented in the literature, leading to a great reduction in the number of references about IRS deployment.
- IRS-deployment-related works are in a preliminary stage, with very simple scenario models to explore basic propagation mechanisms with IRS construction. This stage results in scare reference works and a lack of RT scenario models on IRS deployment under complicated scenarios in high accordance with reality. Even in the most related work, there are some omissions in the simulated model.
- With existing open software, IRS with small sizes are simulated in the literature. However, since the size of IRS plays a significant role in IRS performance, integration of IRS simulation with existing RT simulators can be a problem that required to be tackled.

- There are scarce studies on IRS deployment with RT under a simulated scenario with high reliability. To the best of my knowledge, the first related study utilized an iterative algorithm for all the RT model simulations and calculations. Since RT simulation under a complicated scenario with high resolution requires large computation memory and time, the iterative algorithm to simulate all the deployment possibilities is time-consuming. A more efficient method for IRS deployment is worthy of more investigation.

To tackle the above challenges, this project will contribute in terms of:

- This project constructed a new RT model based on a real scenario in Altair HyperWorks WinProp. To improve the simulated scenario model reliability, a ground truth with real measured data [21] and OSM API [71] are utilized in this thesis work, and modifications on the scenario construction are performed for higher consistency with reality, which takes into account vegetation, irregular shape buildings, and ground reflection additionally.
- To integrate large IRS simulation with WinProp, this project compares realistic EM effects of metal unit cell and of IRS unit cell in CST, and infers optimal IRS deployment based on the RT simulation model with metal plates deployment.
- To decrease the simulation time and memory required in the RT simulator, this project proposed a weighted graph to be caluculated in MATLAB with considering multipath phenomena and IRS reflection loss, which decrease the computation time effectively.

3

SIMULATION MODEL

In this chapter, the model simulations are described in detail, which covers the scenario settings, BS, and reflector simulation in WinProp and CST. To start with, the research framework and simulation workflow in WinProp is introduced in Section 3.1, which presents the overall system structure and processes. Section 3.2 - 3.4 elaborates the simulation of the scenario with the benchmark of TU/e campus, simulation of BS radiation pattern, and simulation of metal reflectors and IRS. Finally, a conclusion is given in Section 3.5.

3.1. RESEARCH FRAMEWORK AND SIMULATION WORKFLOW

3.1.1. RESEARCH FRAMEWORK

This research utilized Altair Feko WinProp to construct the RT simulation and reflector assessment. In order to implement and quantify the coverage improvement after deploying the reflectors into an urban RT simulation scenario, the research framework is established as shown in Fig 3.1.

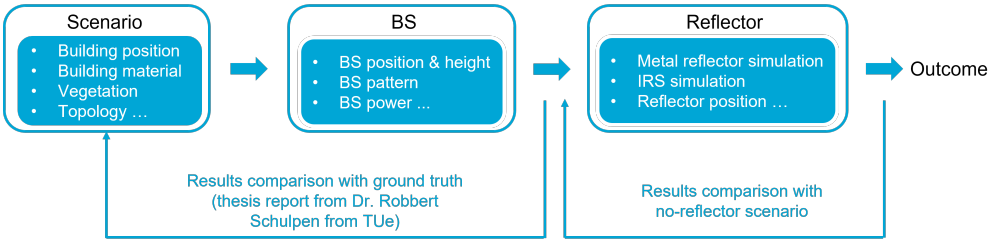

Figure 3.1: Research framework

Within this framework, the reflector deployment underlying RT is carried out by following the three model blocks:

1. *Scenario* (Section 3.2): For the sake of evaluating a real typical urban scenario,

one urban area in the TU/e campus is considered. In this block, the coordinates, material properties, and shape of the buildings and vegetation can be constructed and adjusted to match the real scenario, which leads to shadowing by discrete obstructions, reflections, and diffractions for EM wave propagation. Since the ground reflection also plays a significant role in real signal transmission, the topology will also be considered and constructed in this block.

2. *Base station* (Section 3.3): This block is aimed at designing and deploying the transmitter, the power distribution and wave propagation prediction emitted from which can be computed in WinProp accurately. The BS antenna will be simulated as its antenna pattern instead of importing a real antenna array into the scenario network file. Wave transmission prediction in urban environments is subject to the BS antenna settings (BS position and height, .etc), which could be designed in this block.

   After establishing the scenario and BS, prediction results (power distribution, path loss, delay spread, .etc) can be computed. Then the comparison between the simulated results and the benchmark test results from Dr. Robbert's report [21] will be performed for the scenario and BS validation. This loop will be implemented until the simulated results show good agreement with the ground truth.

3. *Reflector* (Section 3.4): This block is aimed at simulating the reflectors, and this research implements two kinds of reflectors simulation, which is metal reflector and IRS reflector. The metal reflector simulation is executable by simulating as a thin metal cuboid with adjustable position and orientation in WinProp directly, while the IRS reflector simulation is more complicated (Subsection 3.4.1), since to the author's knowledge, no existing RT simulators support IRS simulation. Metal reflector's EM effects make it feasible to treat it as an almost perfect reflector, which is conducive to investigating reflector deployment's effect, and benchmark for the IRS reflector. It is worth pointing out that since all the buildings in WinProp are vertical to the ground [24], this project only considers azimuthal beamforming.

   A loop will be performed here for checking the reflector deployment's effect by comparing the results with different situations (with no reflector, one reflector, two reflectors, .etc). Position and pointing angle of reflectors are the factors investigated in this research, which are tuned for optimal reflector deployment. Finally, after the loop until the optimal deployment, the comparison result will demonstrate the reflectors' improvement in signal coverage.

3.1.2. SIMULATION WORKFLOW

The workflow for the urban propagation simulation is shown in Fig 3.2. In Feko WinProp suite, there are mainly three components: WallMan is used for creating geometry and vector building database, AMan tool enables antenna pattern

production, and ProMan offers wave propagation models simulation and results demonstration. [24]

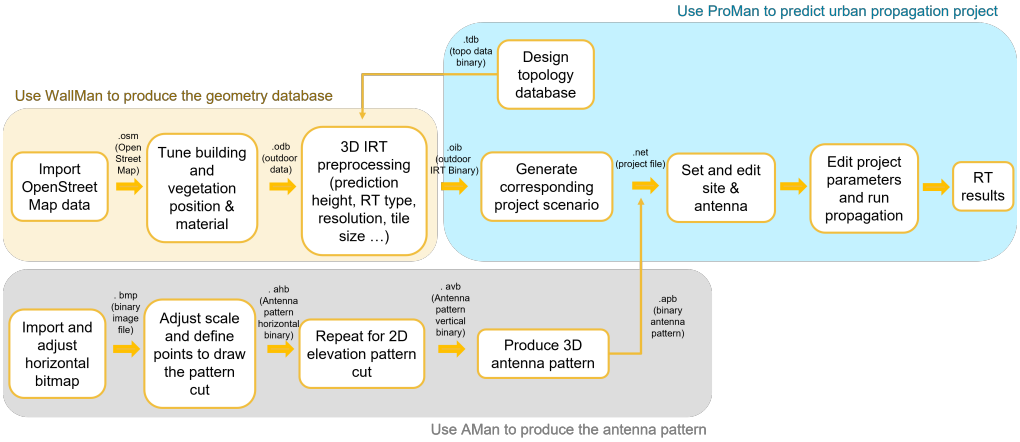

Figure 3.2: Simulation workflow

For the urban RT simulation, according to the three WinProp tools, the workflow steps are as follows:

1. *In WallMan*: To produce the geometry database, the basic exact position and dimension of each building can be done by drawing it in WinProp or importing it from a third-party source. This research investigates scenario construction based on real-world geometry, so in the first step, the building database is extracted from the OSM database [71] (*.osm*), and converted in WinProp format with file extension of *.odb*.

   The imported data from OSM includes coordinates and heights of buildings, but the building material, vegetation (grass, trees, .etc) and hanging bridges are not provided in the basic dataset, on account of which modifications will be tackled in the second step with the benchmark of real scenario from Google map [72] and corresponding descriptions on buildings in [21].

   With the simulated geometry database, the 3D intelligent RT (IRT) preprocessing has to be done for establishing RT visibility relations efficiently by dividing the walls into tiles and edges into segments, which is based on the image-RT approach (Subsection 2.1.1) and is in favor of reducing the computational effort when doing real RT in ProMan. In the preprocessing part, the RT type (2D, 3D, dominant, .etc), prediction height, building discretization, and resolution will be set, which cannot be changed later in ProMan. The topology database (ground elevation) is imported before doing the preprocessing part, which is generated in ProMan. The generated file extension which will be imported into ProMan is outdoor IRT binary file (*.oib*).

2. *In AMan*: For simulating the transmitter, Feko provides real antenna simulation while WinProp AMan is an antenna pattern simulator. In this research with a focus on reflector and RT, AMan is utilized to simulate the transmitter radiation pattern. Exploiting two 2D pattern cuts consisting of horizontal pattern cut and elevation pattern cut, an approximate 3D antenna pattern could be generated in AMan. After importing the pattern image (*.bmp*) as the benchmark, AMan enables to define points to make up a 2D pattern cut (*.ahb* or *.avb*). Finally, a conversion from 2 × 2D pattern cut to 3D Pattern is performed with interpolation.

3. *In ProMan*: This research takes the ground reflection into account. The topology database specifies the ground elevation, based on which the building heights will be superimposed, and the topology database is designed in ProMan.

   Based on the preprocessing outdoor IRT database produced by WallMan, ProMan can generate a new corresponding urban propagation project (*.net*). Then the transmitters with radiation patterns exporting from AMan can be deployed in this scenario. Antenna height, position, power, direction, polarization, .etc modification are executable in this urban project. Next, project parameters are edited, which includes prediction results selection, prediction model selection and its settings, number of interactions, .etc. Finally, the results can be inspected in the ProMan Graphical user interface (GUI).

3.2. PROPAGATION SCENARIO

3.2.1. SCENARIO DESCRIPTION

For the assessment of power coverage with RT in a typical urban scenario, a scenario in the TU/e campus is considered, which can be identified by the geographical coordinates of 51°26′52″ N 5°29′28″ E, with mainly three buildings, trees, grass, open square, and hanging pedestrian bridges comprised in this scenario. Inferred from the figures (Fig 3.3 (a)) provided in the benchmark report [21] and compared with the satellite image (Fig 3.4) illustrated from Google map [72], the selected 28731 m^2 (183m × 157m) area (Fig 3.3 (b)) can be determined and imported from OSM database [71].

As depicted in Fig 3.4, B1, B2, B3, and B4 denote the three buildings, in which the right building is labeled with two parts of B1 and B3 since the structure of it is complicated with different heights. The heights of B1, B2, B3, and B4 are about 41.5m, 17.5m, 12m, and 10m respectively. The surfaces of the buildings are flat and constructed mainly of glass with some metal and concrete, where glass predominates. Inferred from the buildings' characteristics, the three buildings can be identified as a potential reflector [21]. The bridge connecting B2 and B1 is made up of glass as well with good reflection performance. Some trees are distributed in front of B2 and B4, with 9m and 20m heights, respectively. Ground in this region is flat and made up of concrete, covered with fractional grass. For the grass blocks,

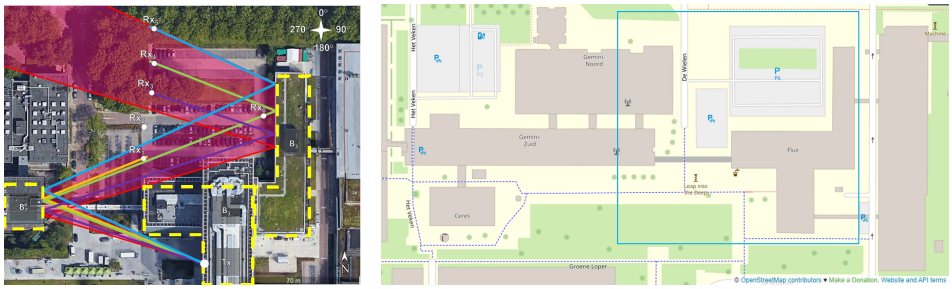

Figure 3.3: (a). The measured scenario in the benchmark [21] (b). Extracted database from OSM [71]

one of the blocks is under the bridge, two of the blocks are distributed parallel in the open square between B4 and B3, and some grass is planted around B1 and B3.

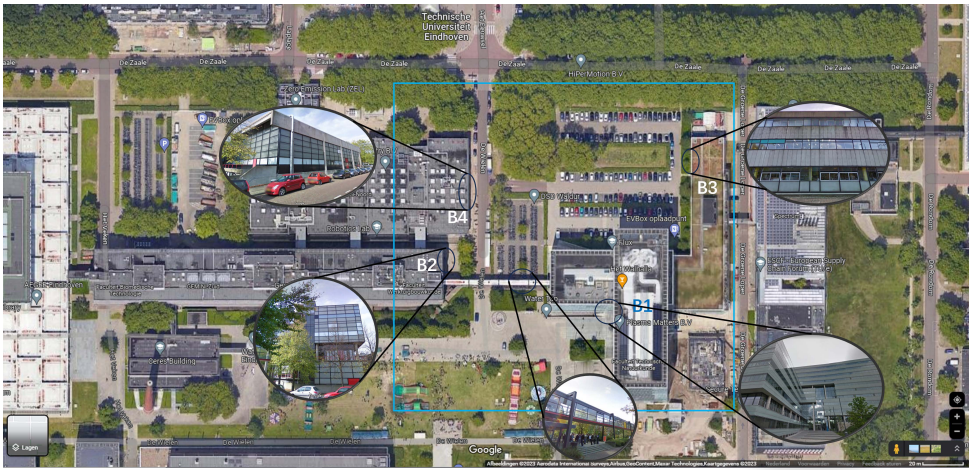

Figure 3.4: The corresponding scenario in Google map [72]

3.2.2. SCENARIO SETTINGS

In WinProp, to save memories [24], the building simulation construction data format is limited by vertical polygonal cylinders with settings of corner coordinates and uniform height, which manifests the simulator does not support building simulation with sloping walls or rugged roofs. There are five types of building simulations provided in WinProp, which are *standard building*, *horizontal plate*, *courtyard* & *towers*, *vegetation buildings*, and *virtual buildings* [24]. This research utilized *standard building* for the three buildings simulation, *horizontal plate* for the pedestrian bridge simulation, and *vegetation buildings* for the trees and grass

simulation. Among those building types exploited in this research, *standard building* and *horizontal plate* are not transparent and have interactions with rays (reflection and diffraction), while rays will go through vegetation with additional attenuation. Furthermore, the material of each building is individual and unitary for the whole building, and most of the corresponding material properties are provided by the WinProp material library.

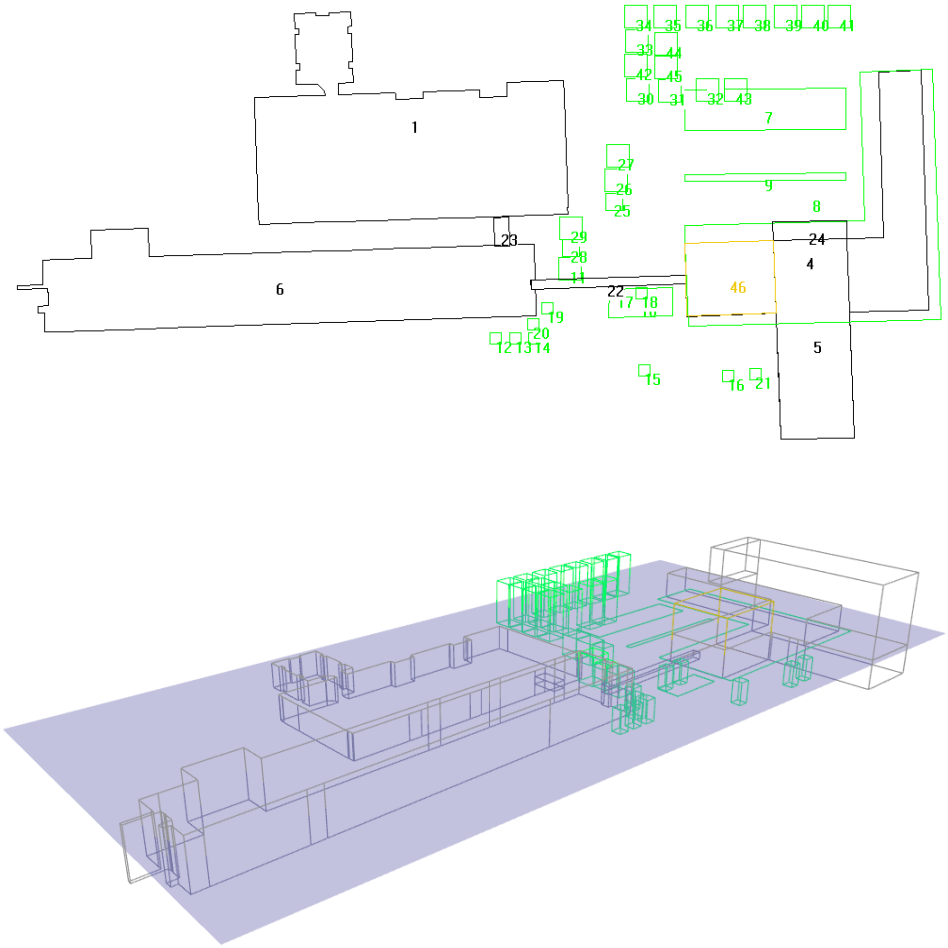

Figure 3.5: (a) 2D top view of the Simulation scenario in WinProp WallMan (b) 3D view of the Simulation scenario in WinProp WallMan

The scenario database exported from the OSM database is incomplete missing some trees, grass, bridge, the height of the buildings, and B1's irregularity, because the initial exported data only provides building corner coordinates according to the top view as seen in Fig 3.3 (b). After modifying the height, position, and construction

of the missing objects in accordance with the research framework (Subsection 3.1.1), the objects simulations in this scenario (Fig 3.5) are established finally as follows:

1. *Ground*: Ground simulation implement is different from other buildings that can be established in WallMan GUI directly, the ground elevation is built in ProMan established in the topology database (Fig 3.2), and the material properties of the ground are set in project parameters when tuning the IRT model setting after selecting the ground reflection.

   According to the demonstration from the satellite image (Fig 3.4), this research implements the ground topology with a flat plane at 0 m, which is comprised of concrete with dielectricity $\varepsilon_r = 6$, conductivity $\sigma = 1.167$ [S/m], permeability $\mu = 1$, reflection loss of 7.51 dB, and surface roughness of 0.3 cm, which are provided from the WinProp material library.

2. *Trees*: Trees are simulated as *vegetation building* cuboids with different sizes and heights, which are inferred by comparing the 3D representations of buildings and the trees in Google map [72]. The size and height of the vegetation cuboids are from 4 × 4m to 8 × 8m, and from 9m to 20m, to simulate the lush foliage. After modifying the tree construction by comparing the path loss distribution with the ground truth [21] as shown in the workflow (Fig 3.1), no tree trunk simulation is implemented finally in this research.

   Since in the material library, the default vegetation properties are for 2000 MHz, which is away from the intended frequency of 28GHz in this research, the vegetation properties are set as additional attenuation of pixels inside of the vegetation with 12 dB, and additional attenuation of rays penetrating the vegetation with 0.07 dB/m [73–75].

3. *Grass*: Utilizing the same vegetation material properties as the trees, the grass simulation is also *vegetation building* cuboids with a height of 0.1m. The distribution of them is according to the relative position provided in the Google map (Fig 3.4).

4. *Building*: The initial imported OSM data provides the rough corners for each building from the top view, more details for each building like the height and the protruding hanging part in B1 (part 24 as shown in Fig 3.5 (a)) are inferred from the engineering drawing [76]. Since the simulator constrains single material for each building, established with *standard building*, the three buildings are made up of 5 mm glass, with relative permittivity $\varepsilon_r = 6$, conductivity $\sigma = 0.0833$ [S/m], permeability $\mu = 1$, reflection loss of 7.53 dB, and transmission loss of 1.97 dB, which are provided from the WinProp material library. Note that indoor prediction is not taken into account in this research, so the thickness has no impact on the ray interaction prediction, and the reflection loss is computed on the interface between air and wall.

5. *Bridge*: Bridge simulation is not supported in WinProp, so this research proposed a new way to simulate bridge approximately. In this research,

the *horizontal plate* is exploited to simulate the bridge and changed the thickness of the material instead of the thickness of the plate to construct the bridge, since WinProp does not support hanging objects with executable object thickness settings. For the bridge between B1 and B2, the position and height are on the basis of the description in the benchmark [21], and the height is from 5 m to 8 m. The material of the bridge is glass, with relative permittivity $\varepsilon_r = 6$, conductivity $\sigma = 0.0833$ [S/m], permeability $\mu = 1$, reflection loss of 7.53 dB, and transmission loss of 2.5 dB. Since the thickness of the pedestrian bridge is simulated by modifying the material thickness, there are only reflections and diffractions on the edges of the bridge, which is constrained by the characteristic of the horizontal plate building type. The protruding hanging part in B1 is also simulated in the same way.

3.3. BS SIMULATION

The transmitters' radiation pattern, position, and height have critical influences on the RT power and path loss prediction. Since commercial antennas do not utilize isotropic antenna to radiate the same power density in all directions, this research simulated a directional antenna radiation pattern as the transmitter. Imported from WinProp pattern examples, the vertical pattern cut and the horizontal pattern cut are shown in Fig 3.6, 3.7. Following the simulation workflow (Fig 3.2), the 3D antenna pattern settled in the simulation scenario is seen in Fig 3.8.

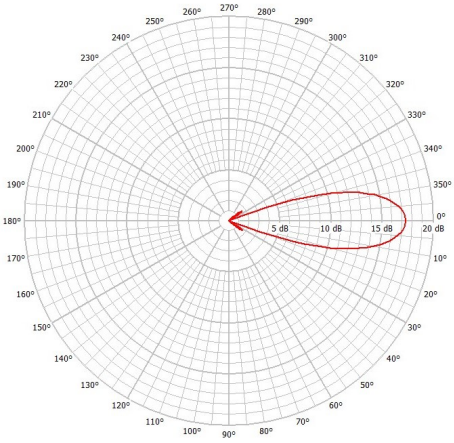

Figure 3.6: Vertical pattern cut

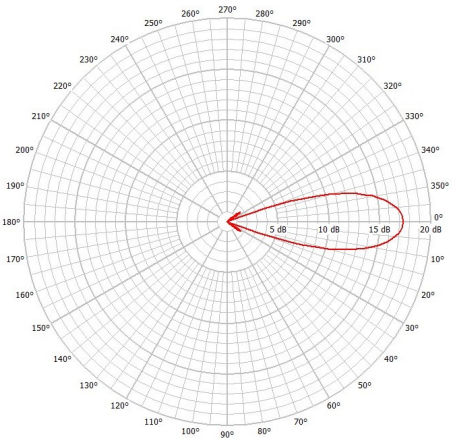

Figure 3.7: Horizontal pattern cut

In accordance with the benchmark [21], the transmitter is deployed on the B1 at a height of 17 m at a frequency of 24 GHz. Fig 3.9 describes the power distribution emitting from the settled transmitter, while the red line indicates the dominant ray from the transmitter to the center of B2, which shows a direct propagation between them. Other BS antenna settings are shown in the table 3.1. Here the frequency of

24 GHz is used for simulation model validation since the benchmark measurement exploited 24 GHz test, while the frequency of 28 GHz is the aim frequency in this research, since 28 GHz is one of the most potent and important bands for 5G [77, 78], whose standardization already has been done [1]. And the simulation model validation under 24 GHz with benchmark [21] forces a reliable scenario model with good agreement to reality (trees position, building material, simulation tile size, etc.), which is dependent on the real scenario and will not be changed with different BS frequency, so the slight change of frequency from 24 GHz to 28 GHz is reasonable, and the scenario model can be applied under 28 GHz directly.

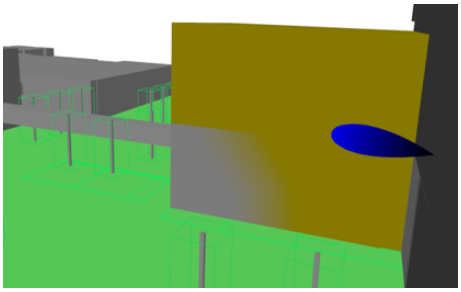

Figure 3.8: 3D antenna pattern settled in the simulation scenario

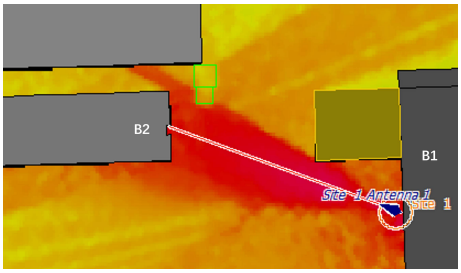

Figure 3.9: Transmitter pattern direction

Table 3.1: BS antenna settings

Tx power	40 dBm
f	24 GHz / 28 GHz
Height	17 m
Gain	17.34 dBi
Polarization	vertical
Azimuth orientation	290°
Downtilt orientation	0°

3.4. REFLECTOR SIMULATION

3.4.1. REFLECTOR SIMULATION PIPELINE

Since no existing simulator supports IRS simulation, how to simulate the reflectors in WinProp is indispensable and challenging. This research simulates two reflectors, which are metal reflectors for investigating the deployment of reflectors in WinProp directly and being regarded as the reflector benchmark to be compared with IRS, and the other one is IRS for realizing 6G with improved coverage.

Fig 3.10 illustrates the reflector simulation pipeline. This research used WinProp,

CST, and MATLAB to tackle the problem of obtaining power distribution under the scenario with IRS.

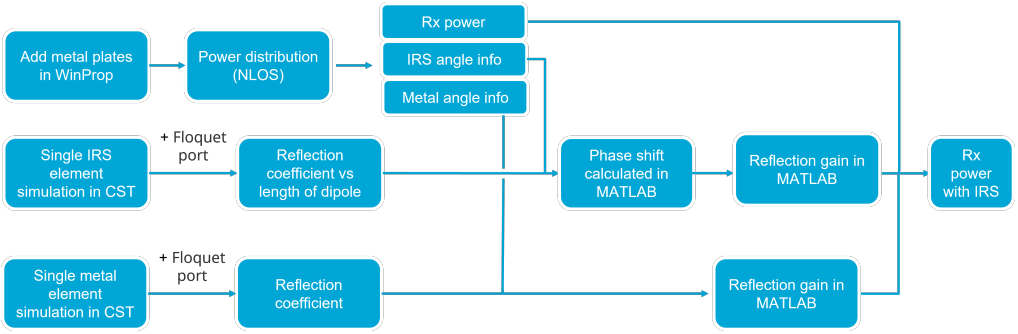

Figure 3.10: The reflector simulation pipeline

1. *Metal plate simulation in WinProp*: It is feasible to simulate the metal plate in WinProp as a *standard building*. With setting the four corner coordinates, heights, and material properties, metal plates with different sizes can be deployed in the simulated scenario. Different corner coordinates lead to different azimuth beamforming, and since building wall bending is not supported in WinProp, elevation beamforming is not considered in this project. Following the simulation workflow (Fig 3.2), the corresponding power distribution can be predicted, with which the receiver point power, IRS angle information, and metal angle information are inferred.

2. *IRS simulation in CST and MATLAB*: IRS is comprised of massive unit cells to passive beamforming cooperatively. Different passive IRS design corresponds to different parameters to realize phase shift adjustment. It is executable to simulate a small amount of IRS elements in CST, but once the number of elements is huge, the simulation in CST requires a mickle computation memory and time.

   To tackle this challenge, this research proposed a new pipeline to combine IRS with RT simulator. Implementing single IRS element simulation in CST with Floquet port as the excitation source, the reflection coefficient can be calculated with the corresponding parameter sweep. Then with the incident angle information (θ_d, ϕ_d, θ_i, ϕ_i) acquired from WinProp, phase shift for the $(m,n)^{th}$ element of the reflectarray is feasible to be calculated in MATLAB with

$$\begin{aligned}\varphi_{m,n} = -k(&X_{m,n}cos(\phi_d)sin(\theta_d) + X_{m,n}cos(\phi_i)sin(\theta_i) \\ &+ Y_{m,n}sin(\phi_d)sin(\theta_d) + Y_{m,n}sin(\phi_i)sin(\theta_i))\end{aligned} \tag{3.1}$$

   where k is the wave number of the incident radiation, $X_{m,n}$ and $Y_{m,n}$ is the x and y coordinates in the n^{th} row and m^{th} column, θ_d and ϕ_d is the desired

azimuth angle and elevation angle, and θ_i and ϕ_i is the incident azimuth angle and elevation angle.

And the reflection gain [79] for the reflectarray is feasible to be calculated in MATLAB with

$$F_{\phi_d,\theta_d} = \frac{1}{MN} \cdot \sum_{m=-M/2}^{M/2} \sum_{n=-N/2}^{N/2} \sqrt{\sigma_{i,r}} \cdot e^{j\varphi_{m,n}} \cdot e^{jk\vec{p}^{\,T}_{m,n}\vec{e_i}} \cdot e^{jk\vec{p}^{\,T}_{m,n}\vec{e_r}} \tag{3.2}$$

where F_{ϕ_d,θ_d} is the normalized reflection gain for the $M \times N$ reflectarray, $\vec{e} = (cos(\phi)sin(\theta), sin(\phi)sin(\theta), cos(\theta))$ is the unit direction vector of the incident and received signal, $\overrightarrow{p_{m,n}}$ is the elements location in the n^{th} row and m^{th} column, $\sigma_{i,r}$ is the reflection gain for a single IRS element at corresponding incident angle and reflected angle, which can be inferred from the reflection coefficient $S_{i,r}$ obtained from CST

$$\sigma_{i,r} = \left|S_{i,r}\right|^2 \tag{3.3}$$

3. *Metal simulation in CST and MATLAB*: With the same size as the IRS element, the metal element simulation is implemented in CST with Floquet port excitation, to calculate the metal element reflection coefficient. The thickness of the metal element is the same as the metal simulation in WinProp. With the incident angle and reflected angle information from WinProp simulation scenario, the reflection gain of the metal reflected array can be calculated. Noted that the angle information of IRS and metal plate is different, since IRS is mounted on the walls that the incident angle and the reflected angle can be different, while the metal plate is tuning the reflected angle by tilting the plate mechanically so that the incident angle and the reflected angle must be the same.

In the end, with the power distribution (P_m) predicted in WinProp under the scenario with deploying metal reflected arrays (metal plate), the reflection gain for IRS (F_{IRS}) and metal reflected arrays (F_m) with the same size, the power distribution under the scenario with settling metal reflected arrays is

$$P_{r\_IRS} = P_m + 10\log_{10} F_{IRS} - 10\log_{10} F_m \tag{3.4}$$

3.4.2. IRS REFLECTOR SIMULATION

IRS element simulation in this research is based on [52], which achieves a linear reflection coefficient phase response and phase variation range of about 360° at 27.7 GHz. Fig 3.11 demonstrates a 4.5 × 4.5 mm single IRS element simulation in CST, which is formed by four layers of foam, bonding film, substrate, and ground, and

parallel dipoles along x and y. The distance and ratio ($\frac{lx_1}{lx_2}$, $\frac{ly_1}{ly_2}$) of the dipoles are adjusted for the optimization of linear reflection coefficient phase response, and the length of $lx_{1,2}$ and $ly_{1,2}$ variation corresponds to phase shift adjustment in V-polarization and H-polarization respectively.

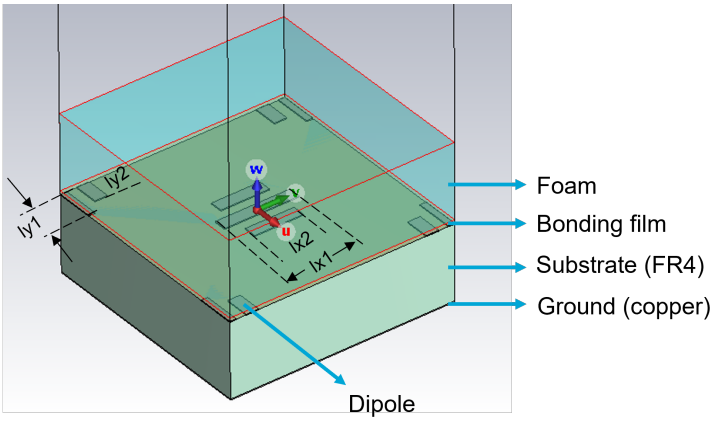

Figure 3.11: IRS element

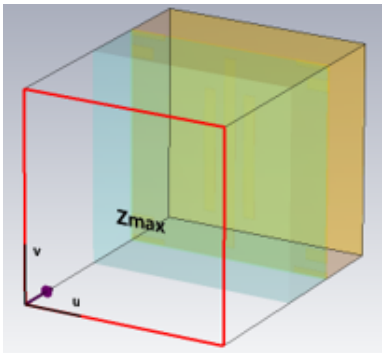

Figure 3.12: Single IRS element with Floquet port

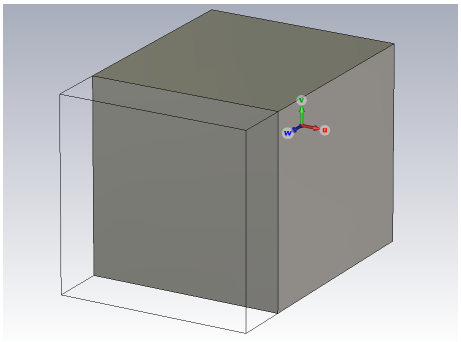

Figure 3.13: Single metal unit cell in CST

To simulate the large-scale IRS, the Floquet port is utilized as the excitation, as shown in Fig 3.12. For establishing periodically expanded boundaries in the corresponding direction and work similarly to modes of a waveguide port, the surrounding boundaries are set as "unit cell", and one "open (add space)" boundary is set perpendicular to the "unit cell" boundaries. With the ground plane, the "electric $E_t = 0$" boundary condition is assigned on Zmin. Noted that glass background simulation for consistency with WinProp reflector installment simulation

is not feasible, since the glass thickness has no impact on the ray interaction prediction.

3.4.3. METAL REFLECTOR SIMULATION

Metal simulation is implemented in WinProp as a metal plate, and in CST and MATLAB as a metal reflected array consisting of a number of metal elements.

In CST, the single metal element is simulated as seen in Fig 3.13 with the material of PEC, in which the thickness of 10 mm corresponds to WinProp metal plate simulation, and the size of 4.5 × 4.5 mm corresponds to IRS unit cell size.

In WinProp, the metal reflector simulation is feasible to be constructed as *standard building* with four corners and perpendicular to the ground, as shown in Fig 3.14, and the top view of the reflector is shown in the upper left corner of the figure. Since this research only considers the passive beamforming in horizontal view (azimuthal beamforming), the height of the metal plate is kept at 10 m which is the *standard building* height by default. By adjusting the coordinates of the four corners, the thickness and the facing direction of the metal reflector can be modified. This research sets 0.01 m as the thickness of the metal reflector and utilizes 1 mm metal material from the WinProp material library.

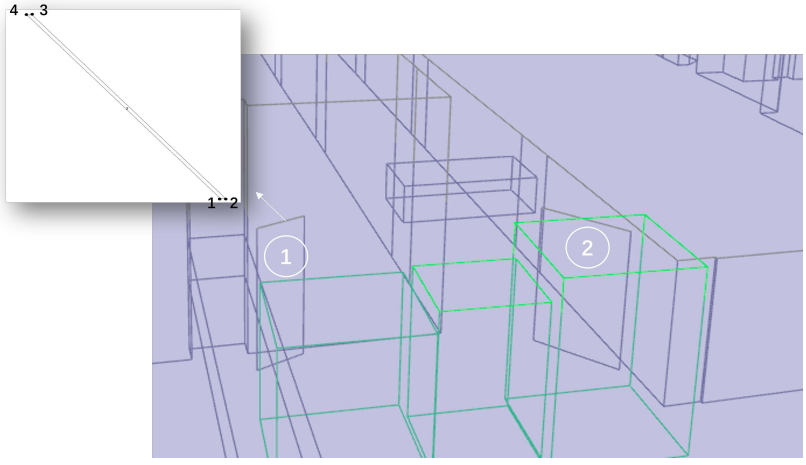

Figure 3.14: Two metal reflector simulation with four corners in WinProp

3.5. CONCLUSION

This chapter mainly elaborates on the model simulation including the research framework with three model blocks, the simulation workflow in Altair Feko WinProp,

and scenario, BS, and reflector simulation. The key points and solved problems are summarised below.

- Based on measured data [21], a new ray-tracing complex simulation scenario is built and modified, with optimization of position, structure, and material of objects (buildings, grass, .etc) in the scenario, parameters and properties in the simulation processing, and BS simulation properties (beamwidth, direction, .etc).

- I proposed a new way to simulate the bridge in WinProp, which is not supported in this simulator. To the best of my knowledge, there are no related works simulating hanging objects in urban scenarios with existing RT simulators for IRS-related problems. This research simulated the bridge as a *horizontal plate* and modified the thickness of the material instead of the thickness of the plate to simulate the sealed glass pedestrian bridge with some heights.

- To the best of my knowledge, this is the first work considering ground reflection and vegetation attenuation close to reality in the investigation of IRS deployment in urban scenarios with existing RT simulators. Since ground reflection and vegetation attenuation are indispensable interactions in ray propagation in reality, this research simulated ground reflection by topology construction and properties adjustment, and simulated trees and grass as *vegetation* blocks and modifies the size, properties, and existence of tree trunks.

- The problem of combining the IRS simulation with RT simulator has been solved, by comparing the reflection gain of the IRS array with the reflection gain of the metal reflector array calculated from MATLAB, which facilitates the connection between IRS power distribution and metal plate power distribution predicted in WinProp.

- The problem of huge simulation time and memory requirements in IRS CST simulation is tackled. The reason for the problem is the massive number of elements consisting in the IRS array, and the long distance from the source to the IRS array, with the requirement of a far-field source.

- The new method to compare metal reflectors with IRS under realistic EM effects decreases the IRS deployment computation time, since with different incident angles and desired reflected angles, some parameters (each dipole length) in the passive IRS array structure should be changed correspondingly, which increased simulation time in CST.

4

MODEL SETTINGS AND VALIDATION

This chapter introduced the parameter settings in RT processing and the simulation results for the model validation compared with the measured data [21]. Section 4.1 introduced the simulation processing parameter settings first. Then Section 4.2 demonstrates the RT prediction model validation and IRS unit cell validation comparing with the measured data [21, 52]. And Section 4.3 concludes the key points finally.

4.1. PROCESSING PARAMETER SETTINGS

Besides object characteristics adjustment, the processing parameters are of vital significance as well, for the sake of model modification in good accordance with reality. In this research, there are two important parameters having a noteworthy influence on the results, which are modules (coherent/incoherent) for the received power, and the other one is the subdivision of reflection and diffraction wall tiles.

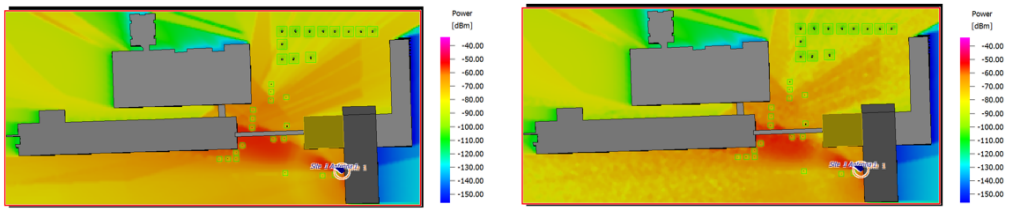

(a) (b)

Figure 4.1: (a). RT power distribution with incoherent ray superposition (b). RT power distribution with coherent ray superposition

For the RT prediction in WinProp, the received power is calculated by the superposition of contributions of different rays [24]. The received power module indicates the coherence of the superposition, which corresponds to the consideration of phases. Fig 4.1 demonstrates the power distribution with incoherent or coherent

superposition, where the color spots manifest the constructive or destructive interference among rays reaching the area. This research investigates EM wave RT simulation based on the real scenario, on account of which coherent module is utilized in the simulation.

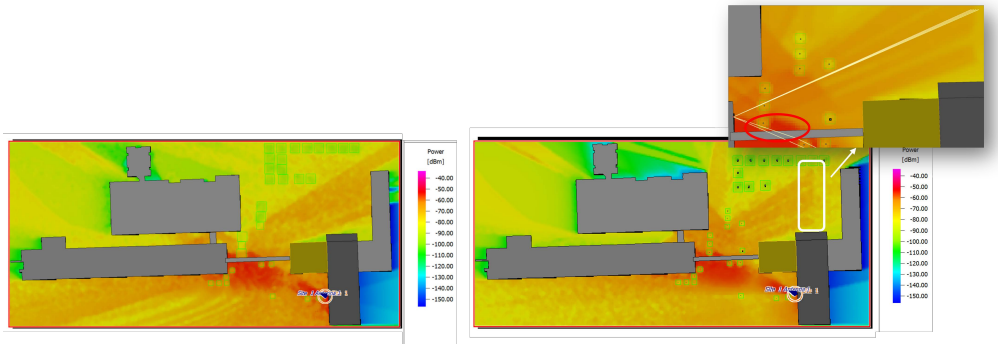

Figure 4.2: (a). Power distribution with 1m × 1m tiles (b). Power distribution with 100m × 100m tiles

As introduced in Subsection 2.1.1, in the image-RT approach, building walls and wedges are divided into tiles for the determination of ray visibility. It is worth noting that the tile size is not the power distribution resolution, but the maximum size of the tiles on the walls and wedges, and they will be handled as the whole wall or wedge if a wall or wedge is smaller than the value [24]. Smaller size value of tiles results in longer computation time and memory. Fig 4.2 shows the power distribution with 1m × 1m tiles and with 100m × 100m tiles (by default). An obvious sharp stratification occurs in the power distribution with 100m × 100m tiles. By observing the dominant rays reaching the boundary, the bridge blockage leads to the stratification, which illustrates the influence of tile size which determines the effect of building blockage and shadows, and large tiles induce small resolution of tile visibility.

After modification, other processing parameter settings are shown in the following table 4.1.

4.2. Model Validation

4.2.1. Scenario Model Validation

In [21], the researcher explored six receivers in the scenario and measured the path loss separately. Since there is no specific location of the receivers and BS provided in the measurement, this research infers the locations based on Fig 3.3 (a).

Table 4.1: Processing parameter settings

Prediction resolution	1 m
Subdivision of walls (reflection) horizontal	1 m
Subdivision of walls (reflection) vertical	1 m
Subdivision of wedges (diffraction) horizontal	1 m
Subdivision of wedges (diffraction) vertical	1 m
Multiple interactions between objects	Yes
Additional prediction planes	surface of buildings
Max number of total interactions	3
Max number of reflections	3
Max number of diffractions	1
Breakpoint distance	20000 m
Max path loss of rays	200 dB
Max number of paths per pixel	20
Superposition of contributions	coherent

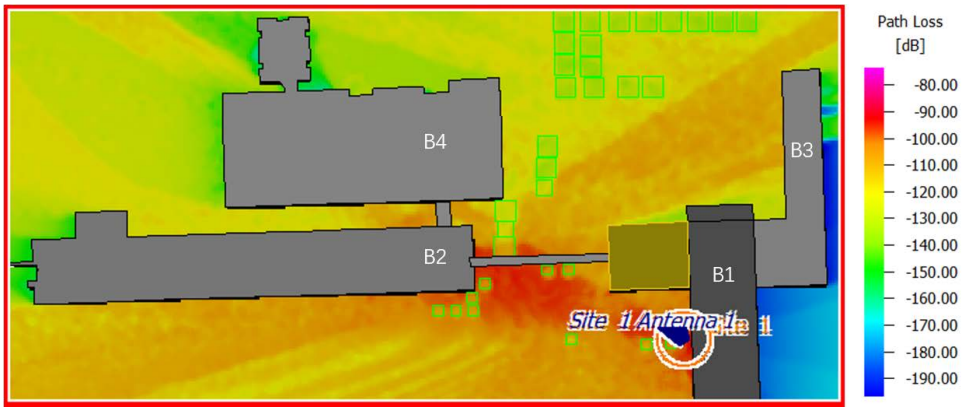

Figure 4.3: Path loss distribution with modified parameters

After parameters and object modification, Fig 4.3 demonstrates the path loss distribution with RT prediction. It is observed that B1 leads to obstructions that a shadowing green area is formed above B1. Additionally, the pedestrian bridge causes an obstacle as well which leads to a sharp red-orange stratification between B2 and B4. Reflected following Tx - B2 - B3 - the woods, an obvious reflection path is seen in this power distribution, which shows good agreements with reflection path analysis in Fig 3.3 (a). Fig 4.4 demonstrates the first 4 level rays for Rx 1 and Rx5. With green points representing diffractions and red ones representing reflections, and the color of rays corresponding to the path loss color bar, the dominant ray for Rx1 and Rx5 are along reflection from B2 or reflections from B2 and then B3, which

matches the reflection path analysis in Fig 3.3 (a).

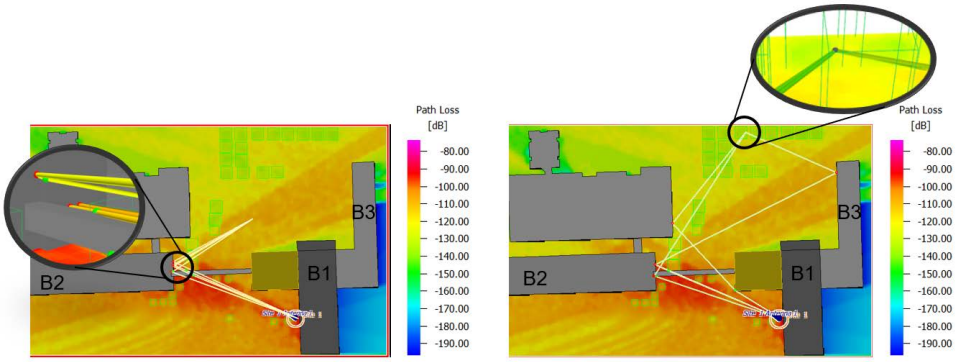

Figure 4.4: First 4 level rays for Rx1 and Rx5

Exploring path losses at each receiver position, Fig 4.5 indicates the comparison between the path losses in simulated data and measured data. It is seen that except for Rx2 (5.3% error), at all Rx positions, the path losses of simulated data show good accordance with the real measurement. The reason for the difference can be BS beamwidth or other flexible scenario reasons in real measurement. The trend in the line chart not only evinces the blockage and reflection of buildings, but also quantifies the attenuation influence of vegetation, which results in the high path loss at Rx3 and Rx5.

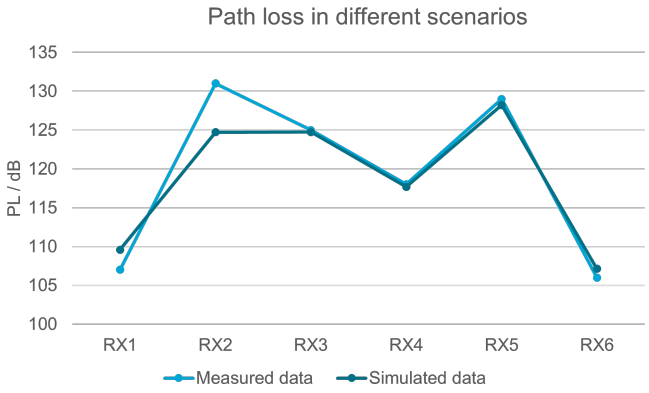

Figure 4.5: Path loss validation with measured data

4.2.2. REFLECTOR MODEL VALIDATION

Based on the IRS simulation pipeline as shown in Fig 3.10, a single IRS unit cell (Fig 3.11) is simulated referring to [52]. After simulating the IRS unit cell with different lengths of lx from 1.5 mm to 4 mm for vertical polarization wave, Fig 4.6 shows the amplitude response and phase response with incident wave theta angle of about 50 degrees and phi of 175 degrees. It is observed that the amplitude response is kept at about -0.3 dB with dipole lengths of 1.5 mm to 2.7 mm, and the dielectric losses are below 1 dB for most of the dipole lengths, which matches the performance in [52]. A smooth phase variation can be seen in the S parameter phase response, covering about 360° phase range after unwrapping.

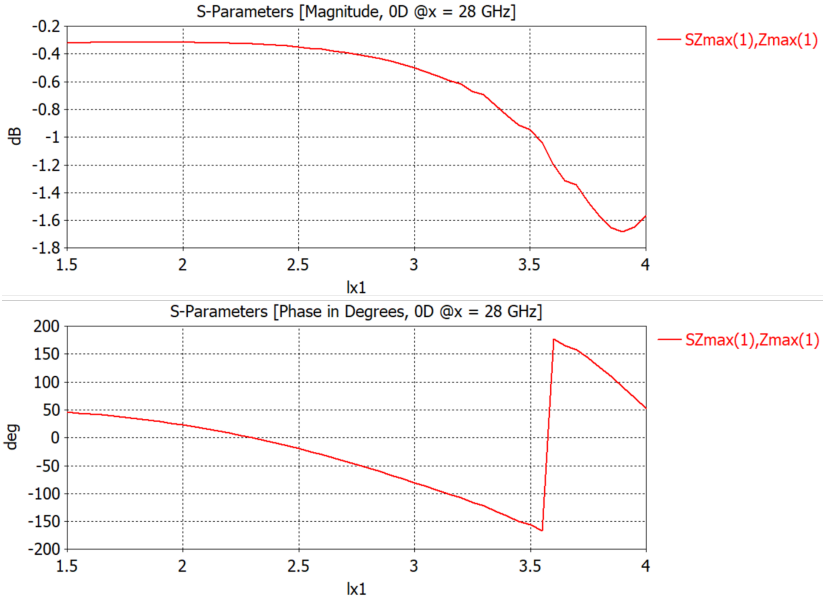

Figure 4.6: Amplitude response and phase response for IRS unit cell reflection coefficient

For the assessment of beamforming of passive IRS, a 4×4 IRS array is simulated in IRS with plane wave excitation. Because of the high requirement of computation memory for large IRS with massive elements, CST does not support simulating a larger IRS array. However, because of the small size of the IRS leading to a huge influence from the edges of the IRS. The inoperability of large IRS simulation in CST evinces the challenge and necessity of how integrating the IRS pattern with RT model, which has been tackled in Subsection 3.4.1.

4.3. CONCLUSION

This chapter explored the parameter settings in RT processing. Then with the built RT scenario model, the scenario and IRS unit cell model validation are assessed. Key

points from this chapter are summarised below.

- Ray superposition module and subdivision tile size are two significant simulation processing parameters for good accordance with reality. This research utilizes coherent ray superposition and 1m × 1m subdivision tile, which shows good consistency between the simulation and measurement, but also leads to long computation time simultaneously.
- Path loss distribution with simulated data shows good agreement with measured data, which demonstrates the high reliability and accuracy of the simulated scenario model. The blockage caused by the hanging pedestrian bridge and the attenuation caused by the trees indicates the indispensability of these object construction when investigating RT simulation or IRS deployment, which are not considered in other research, to the best of my knowledge.
- The scenario validation comparing with the benchmark [21] demonstrates the 5.3% maximum error (RX2) in path loss, and the IRS unit cell validation demonstrates a smooth phase response covering about 360° phase range after unwrapping. The validations show good performance of the models.
- The robust amplitude response and smooth linear phase response of the IRS unit cell indicate the feasibility of utilizing this IRS element model for passive beamforming by adjustment of the appropriate dipole length.

5

IRS DEPLOYMENT

This chapter introduces model optimization with problem formulation, and transformation of the problem into a weighted graph. Section 5.1 elaborates on the problem and the weighted graph first. In Section 5.2, the deployment optimization solution is detailed. Finally, conclusions and key points are drawn in Section 5.3.

5.1. DEPLOYMENT OPTIMIZATION PROBLEM FORMULATION

There are many open areas contained in this urban propagation scenario served by the transmitter located at B1, which could be the "candidate" position of a receiver. However, for the selection of a RoI, it is important that it is in NLOS areas, hard to reach only with interactions on buildings, and it is possible to reach with reflectors. Adhering to this constraint of RoI selection, the 40 m × 10m RoI is selected between B1 and B3 as shown in Fig 5.1. Furthermore, reflector surface placement selection cannot be arbitrary as well, and the constraint is that reflectors are mounted on one facade of a building wall in a LOS area from Tx or from other reflectors. Accordingly, the three "candidate" surface positions (S1, S2, S3) are selected as shown in Fig 5.1.

Owing to the positions of the "candidate" walls, Tx, and RoI, the optimization problem is constructed as a weighted graph (Fig 5.2), in which each link represents a set of ray possibilities (I) with a start node and terminal node, having a heterogeneous weight. Radiated by the source, the EM wave can reach the three "candidate" reflectors in direct or indirect paths without any additional reflector settling under high power (larger than -75 dBm), which is feasible to reflect again to other places. Once the rays reach the reflector, with adjustment of the reflector azimuth facing angle (angle between S1 and y-axis) in a range of 360°, multiple reflected ray possibilities are demonstrated surrounding each "candidate" building. However, among the miscellaneous ray possibilities, the link will be ended with "no reflector" when the rays reflect into an open area without "candidate" surfaces, while others will connect the surfaces, sources, and RoI with weights. Fig 5.2 demonstrates all the connection possibilities. Based on the propagation weighted graph, the optimal problem is the IRS position optimization on each "candidate" wall in each link, which can be assessed by weight.

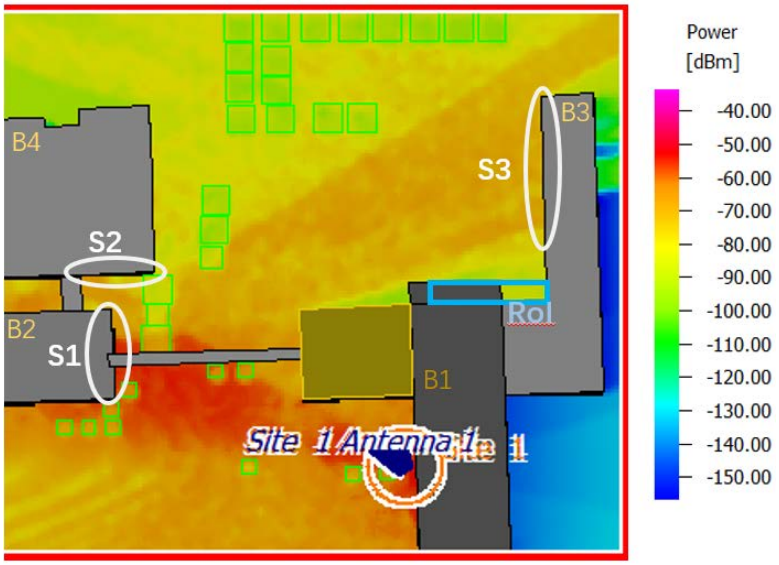

Figure 5.1: Simulated scenario with selected RoI and "candidate" building walls

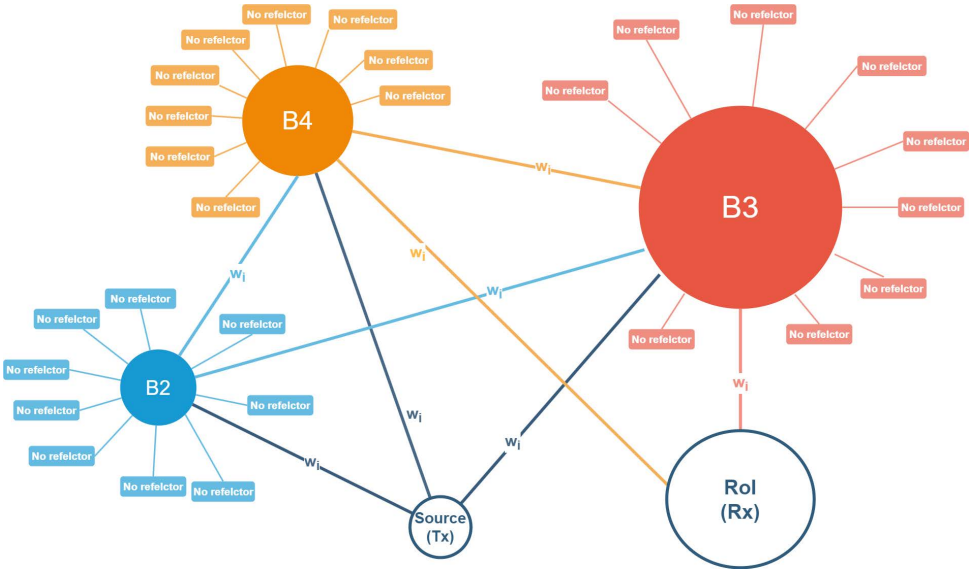

Figure 5.2: Ray propagation weighted graph

5.2. DEPLOYMENT OPTIMIZATION

5.2.1. ANGLE RANGE SELECTION

In this research, the position of S1 on B2 is fixed, since it is in the LOS area from the source with high received power. With size of 2m × 10m × 0.01m in which the height of 10m is by default, S1 reflects waves to B3 or B4. The angle range for the S1 and corresponding next reflector positions are explored by the recursive dichotomy. More in detail, three reflector positions are investigated first, then if two of them lead to an extreme desired situation in a desired area than the other one, another reflector will be installed in the center of the two reflectors.

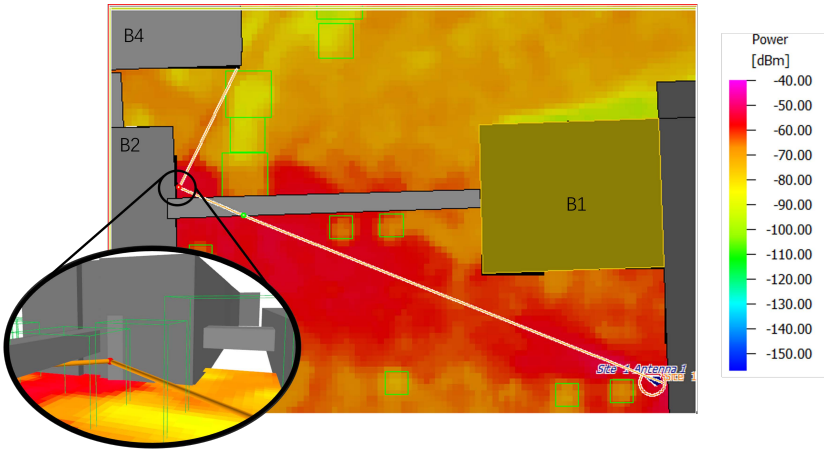

Figure 5.3: Power distribution with S1 facing to right B4

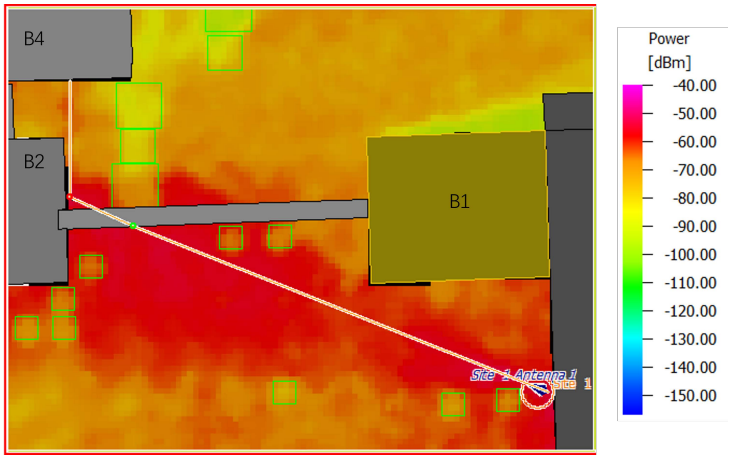

Figure 5.4: Power distribution with S1 facing to left B4

Fig 5.3 and Fig 5.4 demonstrate the power distribution with different S1 azimuth angles for reflecting to B4. It is seen that reflection rays are emitted from S1 to B4 "candidate" wall with high power (about -70 dBm). Thus, because of the blockage of B2 and edge of B4, for the link from B2 to B4, the S1 azimuth facing angle range can be 20.85° to 33.91°.

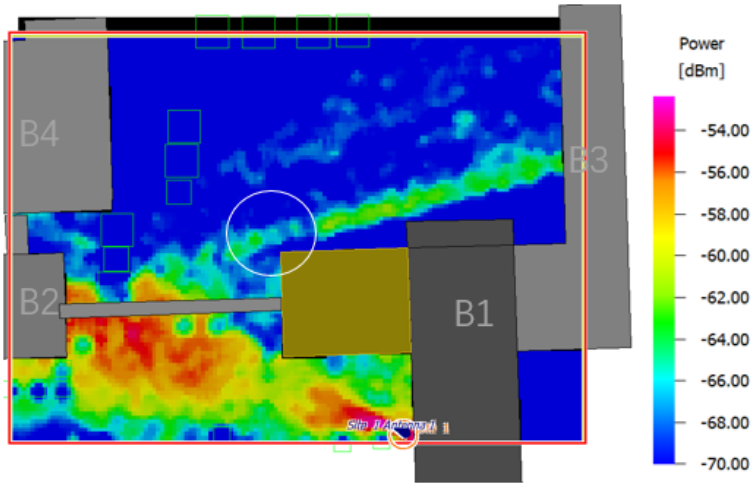

Figure 5.5: Power distribution with S1 facing to B3 with tangential to the corners of B1

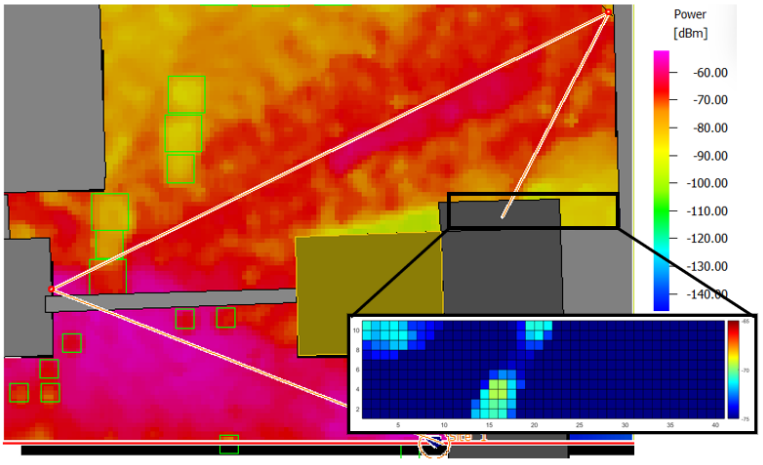

Figure 5.6: RoI Power distribution with S1 facing to further area on B3

Fig 5.5 demonstrate the power distribution with S1 azimuth angles for reflecting to S3. In this figure, a reflected ray radiated from S1 is tangential to the corners of B1, which corresponds to the S1 azimuth angle of -3.6684°. Modifying the metal reflector facing to a further area on B3, and installing the corresponding reflector on B3, the RoI Power distribution is predicted as shown in Fig 5.6. It is observed that few power reach the RoI with about -73 dBm, which corresponds to S1 azimuth angle of 1.7588°. Thus, for the link from B2 to B3, the S1 azimuth facing angle range can be -3.6684° to 1.7588°.

5.2.2. OPTIMIZATION SOLUTION

To solve the reflector deployment optimization problem of optimal position selection in each link in Fig 5.2 to fulfill the largest coverage improvement, an innovative weight calculation for each link is applied by implementing the weight exploration block diagram as shown in Fig 5.7.

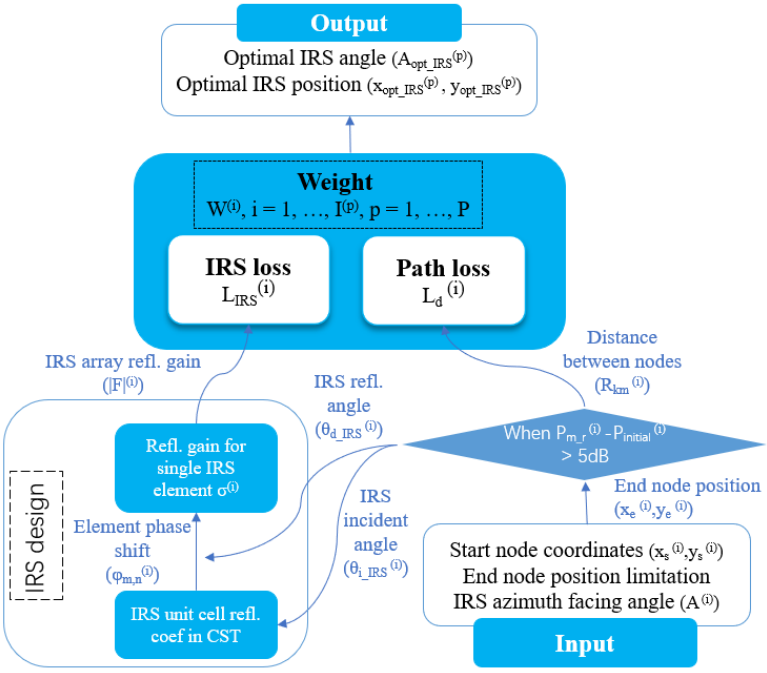

Figure 5.7: Weight exploration block diagram

In a weighted graph with heterogeneous P links, the optimization task can be quantified by properly defining the weight $\{w^{(i)}; i = 1, ..., I^{(p)}; p = 1, ..., P\}$, where I is the total number of path possibilities in p^{th} link (from S1 to S2, etc.), and the

optimal path is the one with the largest total weight. It is worth pointing out that the weight here is used to compare path feasibility in one link, instead of calculating the true received power.

Underlying the free space path loss for one path eliminating atmosphere, rain, and antenna effects [80], the path loss is defined as follows

$$L_p^{(i)} = 20\log_{10} R_{km}^{(i)} + 20\log_{10} f_{MHz} + 32.44 - 10\log_{10} |F|^{(i)} \tag{5.1}$$

where $R_{km}^{(i)}$ is the distance between the start node and ending node in $i^{(p)th}$ path, f_{MHz} is the center frequency utilized in this simulation, and $|F|^{(i)}$ is the IRS reflection loss with i^{th} incident angle and desired reflected angle.

The received power for the path at the corresponding end node through the following expression:

$$P_r^{(i)} = P_t - L_p^{(i)} \tag{5.2}$$

where P_t is the Tx power. Since the obstructions, reflections, and diffractions induce multipath phenomena in this simulated scenario, $P_r^{(i)}$ represents the power carried from the ray reflected from the additional reflectors.

In the same link with the same start node and terminal node, the rays have the same P_t, f_{MHz}, and 32.44, on account of which underlying the physics and fulfillment of IRS reflection constraint, the mathematical weight is formulated by

$$\begin{aligned} w^{(i)} &= L_{IRS}^{(i)} + L_d^{(i)} \\ &= 10\log_{10} |F|^{(i)} - 20\log_{10} R_{km}^{(i)} \end{aligned} \tag{5.3}$$

where $L_{IRS}^{(i)}$ is the IRS reflection loss for different desired IRS reflection angles and incident angles, $L_d^{(i)}$ is the wave propagation loss corresponding to the $i^{(p)th}$ path distance from the start node to ending node.

With the formulated weight, there are five blocks in the weight exploration diagram (Fig 5.7), which is also the processing pipeline in MATLAB:

- *Input*: To calculate the corresponding ending node position, the input would be the start node coordinates ($x_s^{(i)}$, $y_s^{(i)}$), and end node position limitation which depends on the position and length of corresponding "candidate" building wall. As shown in Fig 5.1, S1 "candidate" building wall is in the LOS area from the Tx, on account of which the position of S1 is fixed, and thus in the path with S1 node (e.g. Tx-S1-S2-Rx), the considered weight could not include Tx-S1, since this link is the same for all the path possibilities in

Tx-S1-S2-Rx. In one link with different path possibilities, the variable is the start node reflected surface azimuth facing angle with a step of 1°, leading to rays reflected from the surface in different directions. With the input dataset, it is executable to calculate the corresponding IRS incident angle $\theta^{(i)}_{i\_IRS}$, corresponding IRS reflection angle $\theta^{(i)}_{d\_IRS}$, distance between two nodes $R^{(i)}_{km}$, and end node positions$(x^{(i)}_e,\ y^{(i)}_e)$.

- *Comparison*: To assess the IRS deployment necessity, with the calculated end node positions$(x^{(i)}_e,\ y^{(i)}_e)$, the received power with metal reflector $P^{(i)}_{m\_r}$ will be computed and compared with initial power $P^{(i)}_{initial}$. Once the difference between $P^{(i)}_{m\_r}$ and $P^{(i)}_{initial}$ is larger than 5 dB, then the reflected path from the reflector can be seen as a dominant ray [35], then it is worthy to consider this IRS deployment and weight. Note that because of the coherent ray superposition in RT simulation, initial power at each ending node is calculated by average power in a 3m × 3m area with the center of each corresponding ending node.

- *IRS design*: The IRS design block is based on the IRS simulation pipeline shown in Fig 3.10. Utilizing the input of IRS incident angle $\theta^{(i)}_{i\_IRS}$, the IRS unit cell reflection coefficient vs dipole length is feasible to simulate in CST. After exporting the reflection coefficient into MATLAB and combining it with the phase shift equation 3.1 and reflected angle $\theta^{(i)}_{d\_IRS}$, the reflection gain for a single IRS element $\sigma^{(i)}$ can be calculated with accordance to the corresponding element phase shift $\varphi^{(i)}_{m,n}$. With the reflection gain equation 3.2 and set of IRS array size, the IRS array reflection gain $|F|^{(i)}$ is able to be obtained.

- *Weight*: There are two weights as above-mentioned. For different $i^{(p)th}$ paths, the weight will be calculated accordingly. In one whole link from Tx to RoI, the sum of the weights for each contained path is calculated and compared.

- *Output*: After weight calculation, the optimal path will be inferred after weights comparison, and the outcomes are optimal IRS angle $A^{(p)}_{opt\_IRS}$ and optimal IRS position $(x^{(p)}_{opt\_IRS},\ y^{(p)}_{opt\_IRS})$, and the corresponding IRS four corners coordinates.

5.3. CONCLUSION

This chapter elaborates on model optimization, in terms of reflector deployment optimization, which is tackled by an innovative proposed weighted graph. The key points and solved problems are summarised below.

- Angle range determination is indispensable in saving computation time since the reflector azimuth facing range is 360°, and recursive dichotomy facilitates the angle range determination, which saves simulation time by avoiding trying all the deployment possibilities. Once the propagation path is long, the range boundary can not be the direction facing to other building edges

directly (might meet other obstacles), which is situation-specific and should be analyzed individually.

- To solve and quantify the reflector deployment optimization problem, a weighted graph is designed with the proposed weights formulation, which represents the complicated problem clearly and efficiently and contains all the model uncertainty accurately.
- There are two weights considered in this project, which consider the trade-off between the multipath phenomena and IRS reflection loss for different IRS incident angles and reflection angles. Weights are compared for different whole links instead of calculating layer by layer like a tree, which avoids missing possibilities.
- Calculation time in MATLAB for all the possibilities only requires seconds, resulting in time-saving from simulating all the deployment possibilities in the RT simulator.

6

RESULTS

This chapter elaborates on coverage improvement by establishing reflectors in the scenario, weight validation, and coverage improvement after reflector optimization. Section 6.1 describes the reflectors' deployment influence on the RT scenario. Then Section 6.2 and 6.3 demonstrate the weight validation and coverage improvements by utilizing the proposed deployment optimization approach. Section 6.4 concluded the key points for the model validation, finally.

6.1. RESULTS COMPARISON WITH/WITHOUT REFLECTOR

For the assessment of reflector construction's influence on coverage improvement, Fig 6.1 explored the 1.5 m RT prediction power distribution with or without metal reflectors.

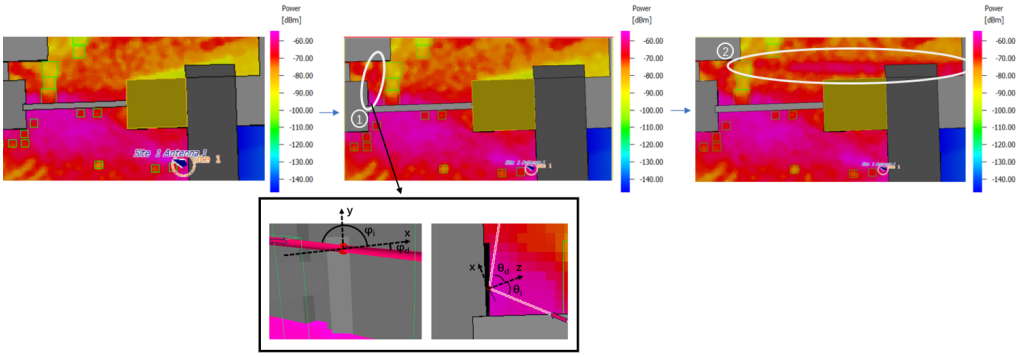

Figure 6.1: (a). 1.5 m power distribution without metal plate (b).1.5 m power distribution with one metal plate (c).1.5 m power distribution with two metal plates

As shown in Fig 6.1 (b) at No. 1, a S1 is deployed between the bridge and B2 with a fixed position since it is covered in the LOS from the Tx. An obvious reflection

path is demonstrated in this simulated scenario, illustrating the effect of reflective surface installment to improve power at the desired destination. Comparing the above-mentioned RoI area above B1 in Fig 6.1 (a) and (b), there are a few coverage improvements in some areas with receiving power from about -100 dBm to -80 dBm. This improvement evinces that as a consequence of the multipath phenomena, reflector installment will lead to power improvement in a large area, not limited to the directly reflected area.

Fig 6.1 (c) describes the 1.5 m power distribution with two metal plates, in which the first reflector is deployed the same as in Fig 6.1 (b). The second reflector at No. 2 is covered in the whole directly reflected path from S1. It is observed in the RoI area, the coverage is highly improved and nearly the receiving powers over the whole area are above -75 dBm.

Based on the metal reflectors deployment in Fig 6.1 (c), the sizes of them, the incident angles, and the reflected angles are inferred accordingly. As a consequence of different beamforming and installment way (i.e. the metal reflectors are mechanically rotated in the simulation setting, while the IRS must lie on the surface of a building), the angle information for metal reflectors and IRS are different. Adhering to the center and size of the metal reflectors, the incident angles, reflected angles, and element numbers of the IRS are determined. With pipeline as shown in Fig 3.10, the size, angle information, and the reflection loss are detailed in table 6.1. It is demonstrated that compared to the nearly perfect metal reflector with high reflection gain, IRS shows good reflection efficiency.

Table 6.1: Details on metal reflector and IRS

	Metal plate 1	**Metal plate 2**	**IRS 1**	**IRS 2**
Size	2 × 10 × 0.01 m	3 × 10 × 0.01 m	444 × 2222	666 × 2222
θ_i**/deg**	51.0421	49.7053	22.1861	10.1019
ϕ_i**/deg**	175	175	175	175
θ_d**/deg**	51.0421	49.7053	79.8981	89.3088
ϕ_d**/deg**	-5	-5	-5	-5
Refl. gain	0.9998	0.9998	0.9003	0.9047

6.2. WEIGHT VALIDATION

To validate the performance of the weight, the link of B2-B4 is assessed. With a fixed reflector S1 on B2 with the center position and with different reflector azimuth angles pointing from the edge of B4 to the due north of the S1 (with the same x coordinates) as introduced in Subsection 5.2.1, the reflector azimuth angles are shifted from 20.85° to 33.91° with a step of 1°. With different reflector azimuth angles, the reflection paths are shown in Fig 6.2. It is shown in the first figure in the first row with reflector azimuth angles of 20.85°, the reflection path (in the white

block) is pointed to the right corner edge of B4, and the reflection path is moved to the left with increasing reflector azimuth angle. Each destination position depends on the S1 position, reflector azimuth angles, and restriction from the B4 wall (the same y coordinates of 5702550.5).

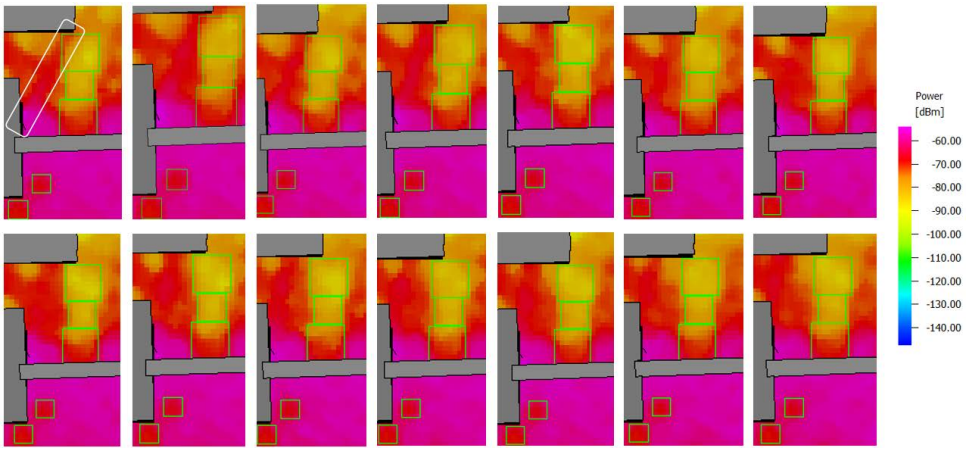

Figure 6.2: Reflection path with 14 different reflectors (with size of 2m × 10m × 0.01m) azimuth angles from 20.85° to 33.91° with a step of 1°, where the first figure in the first row shows the reflection path with reflector azimuth angles of 20.85°, and the rightmost figure in the second row shows the reflection path with reflector azimuth angles of 33.91°

Table 6.2: The corresponding received power with IRS and weight for different reflector azimuth angles

	Path1	**Path2**	**Path3**	**Path4**	**Path5**	**Path6**	**Path7**
Azimuth angle/°	20.8560	21.8560	22.8560	23.8560	24.8560	25.8560	26.8560
P_{r_IRS}**/dBm**	-85.4514	-83.3531	-81.2810	-81.2810	-80.0822	-77.8070	-74.7763
Weight	34.0003	34.1424	34.2718	34.3889	34.4939	34.5873	34.6691

	Path8	**Path9**	**Path10**	**Path11**	**Path12**	**Path13**	**Path14**
Azimuth angle/°	27.8560	28.8560	29.8560	30.8560	31.8560	32.8560	33.8560
P_{r_IRS}**/dBm**	-74.7763	-71.7302	-69.6471	-69.6471	-68.6110	-68.5453	-68.5453
Weight	34.7397	34.7993	34.8479	34.8857	34.9127	34.9292	34.9350

To decrease the influence of incoherent superposition, the received power is calculated by averaging the power in the 3 m × 3 m area around each destination point. Comparing the calculated received power (P_{m_r}) of about -62 dBm with the initial power of about -72 dBm to -86 dBm, the difference between them is much larger than 5 dB, thus the weights can be considered. For the 14 paths with different reflector azimuth angles, the corresponding received power with IRS based

on Fig 6.2 and equation 3.4, and the calculated weight are shown in Table 6.2. It is seen that the two assessment ways both assess Path 14 to be the optimal path, which has the maximum received power with IRS and maximum weight. The results consistency validate the good performance of the weight. However, the differences between each weight do not match each P_{r_IRS}, the reason for which is that in a real RT simulation, there are multi-rays received at one point, and the difference between each ray will be accumulated to a large difference in total, while the weight only considers the only reflection path from additional reflectors. And the initial power containing other rays from multipath ($P_{r\_initial}$) has been compared with the reflection power from the additional reflectors, which means the reflection power from the additional reflectors is the dominant path and the influence from other rays is small. So even though the differences are not very matching, that's reasonable and can exist, and the weight is used for ordering.

6.3. OPTIMIZATION RESULTS

Since some part of the selected RoI area is shadowed by B1 (Fig 5.1) in RT GUI, the initial power distribution data is replotted in MATLAB as shown in Fig 6.3. In the large-area RoI, to calculate the path loss and reflection angles, the RoI is divided into four 10 m × 10 m blocks. In each weight, the initial power is the average power in each 10 m × 10 m block, while the IRS desired reflected angle and the distance is depends on the position of the center of each block.

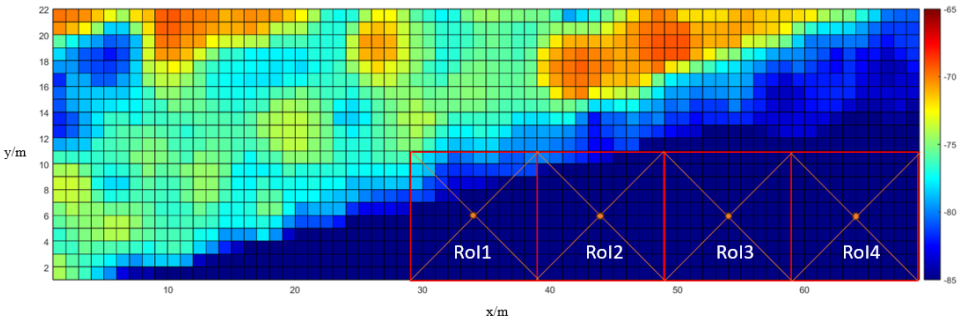

Figure 6.3: Division of the selected RoI into 10 m ×10 m blocks

As an instance, the optimization approach concentrates on the link Tx-B2-B4-Rx, and link Tx-B2-B3-Rx, as shown in Fig 6.4 (a) and Fig 6.5 (a). For the link Tx-B2-B4-Rx, With the S1 angle range constraint (20.85° to 33.91° with a step of 1°) introduced in Subsection 5.2.1 and following the weight exploration block diagram shown in Fig 5.7, as shown in Fig 6.4 (b), in the 14 × 4 path possibilities, the optimal S1 azimuth facing angle is 26.856°, and the corresponding S2 center coordinate is (673076.9925, 5702550.5) with optimal S2 azimuth facing angle pointing to RoI 1

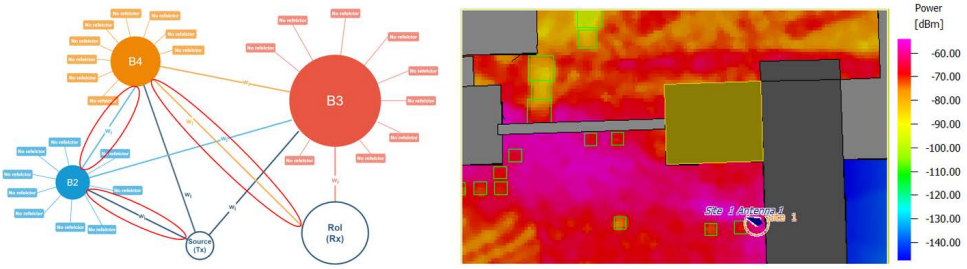

Figure 6.4: (a). Concentrated link with reflection on B2 and B4 (b). Optimal position with two reflectors on B2 and B4

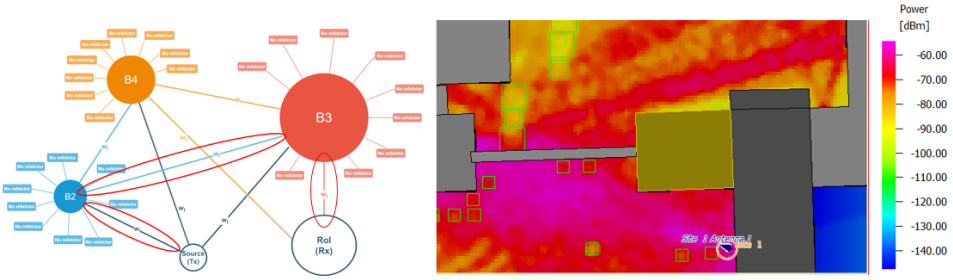

Figure 6.5: (a). Concentrated link with reflection on B2 and B3 (b). Optimal position with two reflectors on B2 and B3

(the most left block in the RoI). For the link Tx-B2-B3-Rx, with the S1 angle range constraint (-3.6684° to 1.7588° with a step of 1°), as shown in Fig 6.5 (b), in the 6 × 4 path possibilities, the optimal S1 azimuth facing angle is -3.6684°, and the corresponding S3 center coordinate is (673192.5, 5702563.5) with optimal S2 azimuth facing angle pointing to RoI 4 (the most right block in the RoI).

Furthermore, the size of S1 is set as 2m × 10m × 0.01m owing to the fact that the prediction resolution in this scenario is 1m, and the size of it should be big enough to reflect high-power rays with minimizing cost and environmental impact. It is observed that with the calculated S2 and S3 center coordinates, the reflector is covered in the reflected area from S1, which modifies the good match of propagation simulation between S1 and S2, S3 in the MATLAB code and RT simulator. The size of S2 and S3 is set as 3m × 10m × 0.01m to reflect all the direct reflected rays from S1.

The division of RoI (Fig 6.3) results in different S2 and S3 reflected angles, and after simulation for each situation, Fig 6.6 (a) demonstrates the power distribution with S2 azimuth angle pointing to RoI1 which is the optimal situation in link Tx-B2-B4-Rx. Fig 6.6 (b) demonstrates the power distribution with S3 azimuth angle pointing to

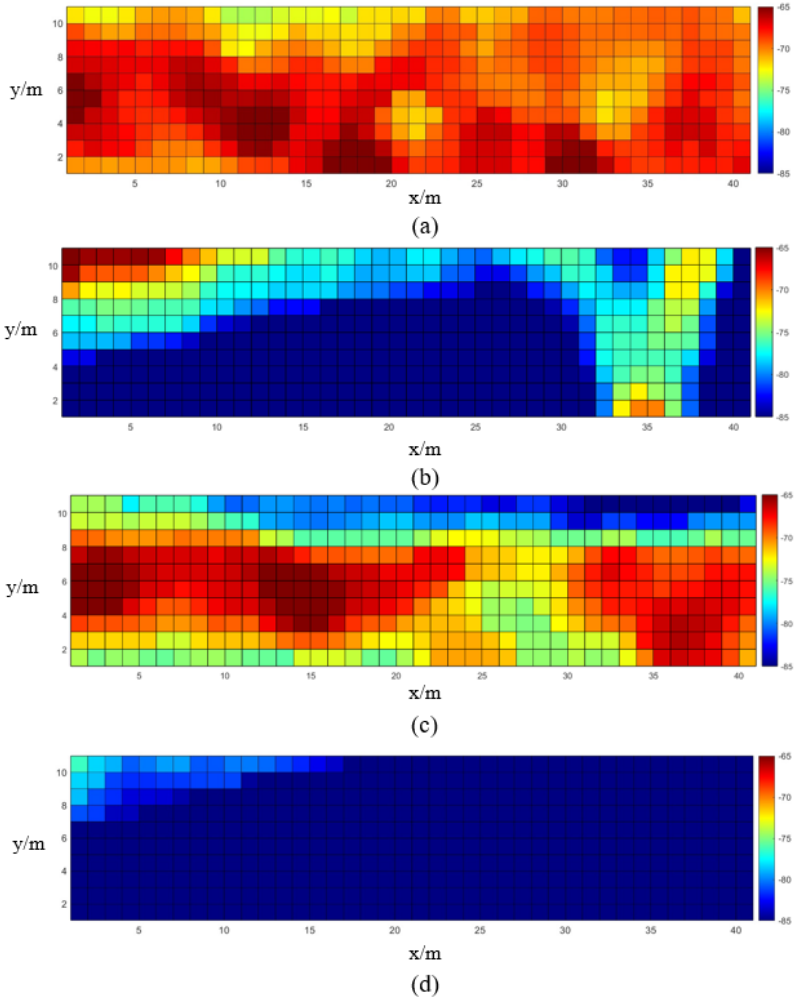

Figure 6.6: (a).The power distribution in RoI under optimal reflector deployment (Tx-B2-B4-Rx) (b).The power distribution in RoI under optimal reflector deployment (Tx-B2-B3-Rx) (c).The power distribution in RoI with arbitrarily selected reflectors (IRS1 angle of 20.856°, IRS2 pointing to RoI1 in Tx-B2-B4-Rx) (d).The power distribution in RoI without reflector

RoI4 which is the optimal situation in link Tx-B2-B3-Rx. Fig 6.6 (c) describes one arbitrarily selected reflector situation (IRS1 angle of 20.856°, IRS2 pointing to RoI1 in link Tx-B2-B4-Rx). Comparison between power distribution in RoI without reflector (Fig 6.6 (d)) and power distribution under reflector deployment (Fig 6.6 (a) (b) (c)) indicates a great extension on coverage. In Fig 6.6 (b), a reflection path is seen with not very high power because of the further distance, which makes it have

even smaller coverage than Fig 6.6 (c). And Fig 6.6 (a) shows the greatest coverage extension.

Table 6.3: The weights for link Tx-B2-B4-Rx

RoI 1

	Path1	Path2	Path3	Path4	Path5	Path6	Path7
Weight	55.8019	55.8595	55.9077	55.9472	55.9761	55.9957	**56.0058**

	Path8	Path9	Path10	Path11	Path12	Path13	Path14
Weight	56.0045	55.9941	55.9749	55.9451	55.9044	55.8539	55.7936

RoI 2

	Path1	Path2	Path3	Path4	Path5	Path6	Path7
Weight	54.7414	54.8094	54.8674	54.9163	54.9542	54.9824	55.0008

	Path8	Path9	Path10	Path11	Path12	Path13	Path14
Weight	**55.0075**	55.0049	54.9933	54.9708	54.9373	54.8939	54.8405

RoI 3

	Path1	Path2	Path3	Path4	Path5	Path6	Path7
Weight	53.7965	53.8727	53.9385	53.9948	54.0399	54.0750	54.1000

	Path8	Path9	Path10	Path11	Path12	Path13	Path14
Weight	54.1132	**54.1168**	54.1113	54.0949	54.0672	54.0295	53.9817

RoI 4

	Path1	Path2	Path3	Path4	Path5	Path6	Path7
Weight	52.9443	53.0272	53.0994	53.1618	53.2127	53.2535	53.2840

	Path8	Path9	Path10	Path11	Path12	Path13	Path14
Weight	53.3024	**53.3112**	53.3108	53.2992	53.2763	53.2434	53.2003

Table 6.4: The weights for link Tx-B2-B3-Rx

RoI 1

	Path1	Path2	Path3	Path4	Path5	Path6
Weight	**46.8065**	46.2605	45.6220	44.8905	44.0840	43.3946

RoI 2

	Path1	Path2	Path3	Path4	Path5	Path6
Weight	**49.2363**	48.3822	47.4424	46.4366	45.3907	44.4973

RoI 3

	Path1	Path2	Path3	Path4	Path5	Path6
Weight	**52.1778**	50.6964	49.2559	47.8651	46.5262	45.4093

RoI 4

	Path1	Path2	Path3	Path4	Path5	Path6
Weight	**54.8465**	52.4584	50.4796	48.7509	47.1892	45.9189

Table 6.3 and Table 6.4 describe the weights for link Tx-B2-B4-Rx and link Tx-B2-B3-Rx separately for four RoIs. In Table 6.3, Path 7, Path 8, Path 9, and Path 9 have the maximum weights for RoI 1, 2, 3, and 4 respectively, and Path 7 pointing to

RoI 1 is the optimal one in link Tx-B2-B4-Rx. In Table 6.4, Path 1, Path 1, Path 1, and Path 1 have the maximum weights for RoI 1, 2, 3, and 4 respectively, and Path 1 pointing to RoI 4 is the optimal one in link Tx-B2-B3-Rx.

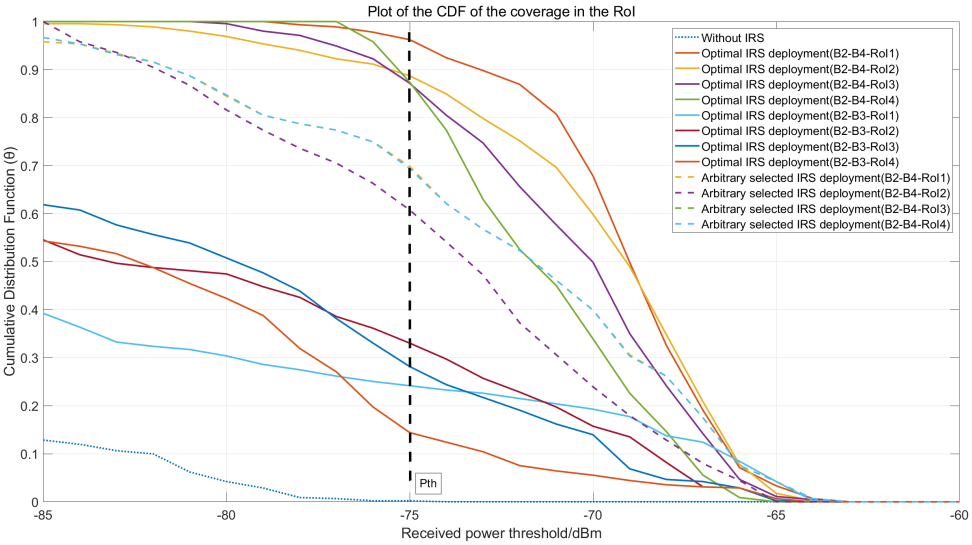

Figure 6.7: The plot of the CDF of the coverage in the RoI under situations with no reflectors, optimal reflectors, and arbitrarily selected reflectors

Fig 6.7 explored the behavior of CDF of the coverage in the RoI under different situations with no reflectors, optimal reflectors for each RoI in the two links, and arbitrarily selected reflectors for each RoI. With the received power threshold from -85 dBm to -60 dBm, it turns out that a declining trend in all the probability functions, and improvement of the wireless coverage with deploying IRS. All the coverage probability functions decrease to 0% when the threshold is -63 dBm.

With the optimal IRS deployment pointing to RoI1 in link Tx-B2-B4-Rx according to the weight, the probability function keeps larger than the other situations, which matches the weight comparison in Table 6.3, and at the threshold of -75 dBm, the coverage probability reaches 96.23% while the coverage probability is almost 0% when no reflectors.

For the optimal IRS deployment pointing to RoI4 in link Tx-B2-B3-Rx according to the weight, the coverage probability only reaches 14.41%, but is smaller than the other 3 paths pointing to other RoI, which is because of the influence of different incident angles into the whole RoI.

Comparing the two links, it is shown that link Tx-B2-B4-Rx works better than link Tx-B2-B3-Rx, even the arbitrary paths for link Tx-B2-B4-Rx have a better performance than the optimal path in Tx-B2-B3-Rx. The comparison between the two links indicates that link selection is also essential. Comparing all the results, the

better selection is the optimal deployment with the path Tx-B2-B4-RoI1, and the weight works well when the considered path has a similar incident angle to RoI or when the area of RoI is not very large as shown in Section 6.2.

6.4. CONCLUSION

This chapter mainly elaborates on the simulation results. To start with, the power distribution results with or without reflectors are discussed, and then the weight validation and coverage improvement with optimal IRS deployment are presented. The key points are summarised below.

- Additional reflector deployment in an urban area facilitates power improvement in a large area, especially in the directly reflected area. And after IRS and metal reflection gain (about 0.99) calculation, IRS shows good reflection efficiency (about 0.9), which makes it feasible to substitute IRS with metal plates in the simulated area for the sake of coverage improvement.
- Weight validation shows a good match with RT simulation with 3m × 3m, which shows its good performance and feasibility.
- With optimal IRS deployment on B2 and B4, a great extension on coverage is shown in the results, with coverage probabilities increasing from 0% to 96.23% with a threshold of -75 dBm, and it works better than a simulation with arbitrarily selected IRS deployment.
- Link selection is also essential that the optimal path in one link might work worse than an arbitrarily selected path in the other link.
- The difference in the performance of weight in the link Tx-B2-B4-Rx with a similar incident angle into RoI and in the link Tx-B2-B3-Rx with a different incident angle into RoI indicates the weight works well when having a similar incident angle to RoI or small area of RoI.

7

CONCLUSIONS AND RECOMMENDATIONS

7.1. CONCLUSIONS

With promising and revolutionizing potential advantages for enhancing the coverage and spectral efficiency in forthcoming wireless communication networks, IRS research sprang up towards hardware impairments, channel estimation, passive beamforming or reflection design, and node deployment. Deployment of IRS in urban scenarios is indispensable for practically exploiting IRS in the advent of the wireless communication revolution, with challenges of limited related studies, no existing simulator supporting IRS simulation, and hard-to-obtain CSI at all locations in reality measurement. To tackle these problems and get the best coverage with optimal reflector deployment, **this research builds a new RT simulation setup with improved reliability based on measured data, first time compares metal reflectors with IRS under realistic EM effects and utilizes it for combining IRS with RT simulation, and proposed a novel, but preliminary, weight graph methodology in improving coverage in NLOS areas by optimal distribution of IRS**.

The main contributions, solved problems, and novelty of the research are summarized below:

- A new RT complex urban simulation scenario is built based on real measured data and a real scenario, with modification of properties of the BS and objects (buildings, grass, .etc) in the scenario, which is introduced in Chapter 3. To solve the problem of simulating hanging objects in an urban simulated scenario and improve simulated scenario reliability, I proposed a new way to simulate the bridge in WinProp by changing the material thickness, and first time considering the vegetation attenuation and ground reflection in IRS deployment in an urban RT scenario close to reality. After validation with the measure data, the RT scenario model accuracy reaches 5.3% maximum error in path loss.

- The problem of combining the IRS simulation with RT simulator has been innovatively solved by the comparison of metal reflectors with IRS under realistic EM effects, which tackled the problem of huge simulation time and memory requirements in IRS CST simulation and IRS deployment computation time in WinProp simulation. The detail of this proposed solution is elaborated in Chapter 3.
- A novel weighted graph is proposed and designed to solve the reflector deployment optimization problem in Chapter 5, which considers multipath phenomena and IRS reflection loss. The proposed weighted graph saves the simulation time from trying all the simulation possibilities. With this methodology, in the instance of the path via B2 and B4 or B3, the coverage is improved from 0 % to 96.23 % with a threshold of -75dBm.

In conclusion, this research designs and provides a new RT complex urban simulation scenario with high reliability, demonstrates the significance of ground reflection and vegetation attenuation which are ignored in other research, and proposes new methodologies for hanging bridge simulation, IRS simulation combination with RT simulator, and reflector deployment optimization.

7.2. RECOMMENDATIONS

Although the IRS deployment problem has been explored and tackled in this research, and the coverage has shown a remarkable improvement, there are some limitations and some recommendations in this research:

- High resolution and small subdivision tile size are significant for precise and reliable RT prediction, however, which leads to long computation time simultaneously. In this scenario, simulating the whole area takes 5 hours on a standard laptop (AMD Ryzen 7 5825U with Radeon Graphics 2 GHz and 16 [GB] for RAM), and 13 hours on TU Delft MS3 server. Simulation with decreasing the prediction area only with the Tx, the reflectors, and the RoI takes 20-30 minutes on the laptop.

  For each path resulting in different IRS angle information, the IRS unit cell phase and amplitude response of the reflection coefficient should be calculated individually. The angle-specific characteristic and three software make it hard to collect data quickly and automatically.

  The constraint of data collection makes it hard to compare path weights quickly and automatically, which constrains the deployment automation.

  To tackle the problem of high computation time requirement in each RT simulation and collect data efficiently, a Gaussian Process and correlation training [81] can be used for weight estimation.

- Constrained by the characteristic of the building type, the proposed bridge simulation only allows reflections and diffractions on the edges of it. Although the validation of path loss with ground truth shows good agreement, the

consideration of the surface reflection of the bridge will increase the model's reliability.

- In a larger-scale deployment scenario, BS deployment would be essential as well. For the problem of BS deployment, take into account the practical space constraints in simulation models, there will be increasing spatial irregularity for the deployment, instead of the conventional grid-based BS deployment model [56]. BS beam steering and the trade-off between optimal deployment of BS and IRS is also one of the key points required to be considered in BS deployment.

- In a larger-scale and more complex deployment scenario with more buildings and vegetation, the low cost and short operating range of IRS lead to a much more dense deployment than active BS or relays, which means a more complicated larger-scale topology for optimization of IRS-aided deployment [12].

  Weight improvement can be considered in the more complex deployment scenario by considering other weights (e.g. vegetation attenuation, number of IRSs, incident angle into the RoI), or with a smaller division of RoI.

  Furthermore, the dense deployment will result in increased interference between the devices [82, 83].

  The Neural Network [66] is a good tool to train the system automatically with the weight input for the selection of optimal reflector positions in a larger-scale deployment scenario.

- This project uses non-reconfigurable IRS to simulate the passive beamforming of IRS in a RT simulator. However, with the limitation of the RT simulator and the differences between reconfigurable IRS and non-reconfigurable IRS, how to integrate reconfigurable IRS with RT and elevation beamforming is still worth investigating.

REFERENCES

[1] B. K. J. Al-Shammari, I. Hburi, H. R. Idan, and H. F. Khazaal. "An Overview of mmWave Communications for 5G". In: *2021 International Conference on Communication & Information Technology (ICICT)*. 2021, pp. 133–139. DOI: 10.1109/ICICT52195.2021.9568459.

[2] H. Zhao, R. Mayzus, S. Sun, M. Samimi, J. K. Schulz, Y. Azar, K. Wang, G. N. Wong, F. Gutierrez, and T. S. Rappaport. "28 GHz millimeter wave cellular communication measurements for reflection and penetration loss in and around buildings in New York city". In: *2013 IEEE International Conference on Communications (ICC)*. 2013, pp. 5163–5167. DOI: 10.1109/ICC.2013.6655403.

[3] I. K. Jain, R. Kumar, and S. S. Panwar. "The Impact of Mobile Blockers on Millimeter Wave Cellular Systems". In: *IEEE Journal on Selected Areas in Communications* 37.4 (2019), pp. 854–868. DOI: 10.1109/JSAC.2019.2898756.

[4] Q. Wu, G. Y. Li, W. Chen, D. W. K. Ng, and R. Schober. "An Overview of Sustainable Green 5G Networks". In: *IEEE Wireless Communications* 24.4 (2017), pp. 72–80. DOI: 10.1109/MWC.2017.1600343.

[5] J. Zhao. *A Survey of Intelligent Reflecting Surfaces (IRSs): Towards 6G Wireless Communication Networks*. 2019. DOI: 10.48550/ARXIV.1907.04789. URL: https://arxiv.org/abs/1907.04789.

[6] L. Liang, M. Qi, J. Yang, X. Shen, J. Zhai, W. Xu, B. Jin, W. Liu, Y. Feng, C. Zhang, H. Lu, H.-T. Chen, L. Kang, W. Xu, J. Chen, T. J. Cui, P. Wu, and S. Liu. "Anomalous Terahertz Reflection and Scattering by Flexible and Conformal Coding Metamaterials". In: *Advanced Optical Materials* 3.10 (2015), pp. 1374–1380. DOI: https://doi.org/10.1002/adom.201500206. URL: https://onlinelibrary.wiley.com/doi/abs/10.1002/adom.201500206.

[7] J. Zhang, E. Björnson, M. Matthaiou, D. W. K. Ng, H. Yang, and D. J. Love. "Prospective Multiple Antenna Technologies for Beyond 5G". In: *IEEE Journal on Selected Areas in Communications* 38.8 (2020), pp. 1637–1660. DOI: 10.1109/JSAC.2020.3000826.

[8] Q. Wu and R. Zhang. "Towards Smart and Reconfigurable Environment: Intelligent Reflecting Surface Aided Wireless Network". In: *IEEE Communications Magazine* 58.1 (2020), pp. 106–112. DOI: 10.1109/MCOM.001.1900107.

[9] Z. Wang, D. Shi, and H. Wu. "The Role of Massive MIMO and Intelligent Reflecting Surface in 5G/6G Networks". In: *2021 International Conference on Wireless Communications and Smart Grid (ICWCSG)*. 2021, pp. 309–312. DOI: 10.1109/ICWCSG53609.2021.00067.

[10] A. Gashtasbi, M. M. Silva, and R. Dinis. “An Overview of Intelligent Reflecting Surfaces for Future Wireless Systems”. In: *2022 13th International Symposium on Communication Systems, Networks and Digital Signal Processing (CSNDSP)*. 2022, pp. 314–319. DOI: 10.1109/CSNDSP54353.2022.9907933.

[11] S. Basharat, S. A. Hassan, H. Pervaiz, A. Mahmood, Z. Ding, and M. Gidlund. “Reconfigurable Intelligent Surfaces: Potentials, Applications, and Challenges for 6G Wireless Networks”. In: *IEEE Wireless Communications* 28.6 (2021), pp. 184–191. DOI: 10.1109/MWC.011.2100016.

[12] Q. Wu, S. Zhang, B. Zheng, C. You, and R. Zhang. “Intelligent Reflecting Surface-Aided Wireless Communications: A Tutorial”. In: *IEEE Transactions on Communications* 69.5 (2021), pp. 3313–3351. DOI: 10.1109/TCOMM.2021.3051897.

[13] Q. Wu and R. Zhang. “Joint Active and Passive Beamforming Optimization for Intelligent Reflecting Surface Assisted SWIPT Under QoS Constraints”. In: *IEEE Journal on Selected Areas in Communications* 38.8 (2020), pp. 1735–1748. DOI: 10.1109/JSAC.2020.3000807.

[14] B. Guo, Y. Wu, M. Yang, and J. Li. “28GHz millimeter wave propagation models based on ray-tracing in urban scenario”. In: *2015 IEEE 26th Annual International Symposium on Personal, Indoor, and Mobile Radio Communications (PIMRC)*. 2015, pp. 2209–2213. DOI: 10.1109/PIMRC.2015.7343664.

[15] M. Y. Kang, J. Y. Lee, and S.-C. Kim. “Analysis of Channel Characteristics for Outdoor 28 GHz Millimeter Wave Channel”. In: *2019 25th Asia-Pacific Conference on Communications (APCC)*. 2019, pp. 388–391. DOI: 10.1109/APCC47188.2019.9026495.

[16] G.-y. Wang, Y.-j. Liu, S.-d. Li, X.-j. Zhang, and Z.-p. Chen. “Study on the outdoor wave propagation at 28GHz by ray tracing method”. In: *2016 IEEE International Conference on Microwave and Millimeter Wave Technology (ICMMT)*. Vol. 1. 2016, pp. 476–478. DOI: 10.1109/ICMMT.2016.7761813.

[17] M. E. Rasekh, A. A. Shishegar, and F. Farzaneh. “A study of the effect of diffraction and rough surface scatter modeling on ray tracing results in an urban environment at 60 GHz”. In: *2009 First Conference on Millimeter-Wave and Terahertz Technologies (MMWaTT)*. 2009, pp. 27–31. DOI: 10.1109/MMWATT.2009.5450459.

[18] Q. Wu, X. Guan, and R. Zhang. “Intelligent Reflecting Surface-Aided Wireless Energy and Information Transmission: An Overview”. In: *Proceedings of the IEEE* 110.1 (2022), pp. 150–170. DOI: 10.1109/JPROC.2021.3121790.

[19] B. Zheng, C. You, W. Mei, and R. Zhang. “A Survey on Channel Estimation and Practical Passive Beamforming Design for Intelligent Reflecting Surface Aided Wireless Communications”. In: *IEEE Communications Surveys & Tutorials* 24.2 (2022), pp. 1035–1071. DOI: 10.1109/COMST.2022.3155305.

[20] X. Tan, Z. Sun, D. Koutsonikolas, and J. M. Jornet. “Enabling Indoor Mobile Millimeter-wave Networks Based on Smart Reflect-arrays”. In: *IEEE INFOCOM 2018 - IEEE Conference on Computer Communications*. 2018, pp. 270–278. DOI: 10.1109/INFOCOM.2018.8485924.

[21] R. Schulpen. “Millimeter-Wave Channel Sounding: Exploring the Wireless Highway of Tomorrow”. English. Proefschrift. - Embargo. - Pdf open access 11-10-2023. PhD thesis. Electrical Engineering, Oct. 2022. ISBN: 978-94-6469-004-0.

[22] T. Geok, F. Hossain, M. Kamaruddin, N. Z. Abd Rahman, S. Thiagarajah, A. Chiat, J. Hossen, and C. Liew. “A Comprehensive Review of Efficient Ray-Tracing Techniques for Wireless Communication”. In: *International Journal on Communications Antenna and Propagation (IRECAP)* 8 (Apr. 2018), p. 123. DOI: 10.15866/irecap.v8i2.13797.

[23] F. Fuschini, E. M. Vitucci, M. Barbiroli, G. Falciasecca, and V. Degli-Esposti. “Ray tracing propagation modeling for future small-cell and indoor applications: A review of current techniques”. In: *Radio Science* 50.6 (2015), pp. 469–485. DOI: 10.1002/2015RS005659.

[24] URL: https://2021.help.altair.com/2021.1.2/winprop/pdf/Altair_WinProp_User_Guide.pdf.

[25] N. Marcuvitz and L. Felsen. *Radiation and scattering of waves*. Prentice-Hall Englewood Cliffs, 1973.

[26] B. Ai, K. Guan, R. He, J. Li, G. Li, D. He, Z. Zhong, and K. M. S. Huq. “On Indoor Millimeter Wave Massive MIMO Channels: Measurement and Simulation”. In: *IEEE Journal on Selected Areas in Communications* 35.7 (2017), pp. 1678–1690. DOI: 10.1109/JSAC.2017.2698780.

[27] M. Gao, Z. Xing, J. Yang, and R. Wang. “Mesurement and Modeling of Indoor Channel Propagation at 28GHz”. In: *2020 IEEE International Symposium on Antennas and Propagation and North American Radio Science Meeting*. 2020, pp. 1231–1232. DOI: 10.1109/IEEECONF35879.2020.9329690.

[28] S. Li, Y. Liu, X. Zhang, and X. Qi. “Measurement and simulation of 28 GHz millimeter-wave propagation characteristics in the corridor environment”. In: *2016 IEEE 9th UK-Europe-China Workshop on Millimetre Waves and Terahertz Technologies (UCMMT)*. 2016, pp. 134–137. DOI: 10.1109/UCMMT.2016.7873988.

[29] B. Neekzad, K. Sayrafian-Pour, J. Perez, and J. S. Baras. “Comparison of Ray Tracing Simulations and Millimeter Wave Channel Sounding Measurements”. In: *2007 IEEE 18th International Symposium on Personal, Indoor and Mobile Radio Communications*. 2007, pp. 1–5. DOI: 10.1109/PIMRC.2007.4394537.

[30] S. Kishimoto, M. Kim, D. He, and K. Guan. “Scattering Process Identification and Cluster Analysis for Millimeter-wave Indoor Channel Model”. In: *2018 International Symposium on Antennas and Propagation (ISAP)*. 2018, pp. 1–2.

[31] M. Dong, W.-M. Chan, T. Kim, K. Liu, H. Huang, and G. Wang. “Simulation study on millimeter wave 3D beamforming systems in urban outdoor multi-cell scenarios using 3D ray tracing”. In: *2015 IEEE 26th Annual International Symposium on Personal, Indoor, and Mobile Radio Communications (PIMRC)*. 2015, pp. 2265–2270. DOI: 10.1109/PIMRC.2015.7343675.

[32] E. M. Vitucci, V. Degli-Esposti, F. Mani, F. Fuschini, M. Barbiroli, M. Gan, C. Li, J. Zhao, and Z. Zhong. “Tuning Ray Tracing for Mm-wave Coverage Prediction in Outdoor Urban Scenarios”. In: *Radio Science* 54.11 (2019), pp. 1112–1128. DOI: https://doi.org/10.1029/2019RS006869. URL: https://agupubs.onlinelibrary.wiley.com/doi/abs/10.1029/2019RS006869.

[33] H. Yi, D. He, P. T. Mathiopoulos, B. Ai, J. M. Garcia-Loygorri, J. Dou, and Z. Zhong. “Ray Tracing Meets Terahertz: Challenges and Opportunities”. In: *IEEE Communications Magazine* (2022), pp. 1–7. DOI: 10.1109/MCOM.001.2200454.

[34] Y. Zhou, Y. Dong, Y. Liu, and X. Sun. “Ray-Tracing Based Multi-Frequency Large-Scale Channel Characterization for Indoor Millimeter Wave Communications”. In: *2020 IEEE 3rd International Conference on Electronic Information and Communication Technology (ICEICT)*. 2020, pp. 211–213. DOI: 10.1109/ICEICT51264.2020.9334243.

[35] Y. Aslan, J. Puskely, A. Roederer, and A. Yarovoy. “Performance Comparison of Single- and Multi-Lobe Antenna Arrays in 5G Urban Outdoor Environments at mm-Waves via Intelligent Ray Tracing”. In: *2020 14th European Conference on Antennas and Propagation (EuCAP)*. 2020, pp. 1–5. DOI: 10.23919/EuCAP48036.2020.9135263.

[36] M. S. Elbasheir, R. A. Saeed, and S. Edam. “5G Base Station Deployment Review for RF Radiation”. In: *2021 International Symposium on Networks, Computers and Communications (ISNCC)*. 2021, pp. 1–5. DOI: 10.1109/ISNCC52172.2021.9615689.

[37] V. H. M. Donald. “Advanced mobile phone service: The cellular concept”. In: *The Bell System Technical Journal* 58.1 (1979), pp. 15–41. DOI: 10.1002/j.1538-7305.1979.tb02209.x.

[38] L. Chiaraviglio, F. Cuomo, M. Maisto, A. Gigli, J. Lorincz, Y. Zhou, Z. Zhao, C. Qi, and H. Zhang. “What is the Best Spatial Distribution to Model Base Station Density? A Deep Dive into Two European Mobile Networks”. In: *IEEE Access* 4 (2016), pp. 1434–1443. DOI: 10.1109/ACCESS.2016.2552981.

[39] J. Kibiłda, B. Galkin, and L. A. DaSilva. “Modelling Multi-Operator Base Station Deployment Patterns in Cellular Networks”. In: *IEEE Transactions on Mobile Computing* 15.12 (2016), pp. 3087–3099. DOI: 10.1109/TMC.2015.2506583.

[40] C.-H. Wang, C.-J. Lee, and X. Wu. “A Coverage-Based Location Approach and Performance Evaluation for the Deployment of 5G Base Stations”. In: *IEEE Access* 8 (2020), pp. 123320–123333. DOI: 10.1109/ACCESS.2020.3006733.

[41] H. Ganame, L. Yingzhuang, H. Ghazzai, and D. Kamissoko. “5G Base Station Deployment Perspectives in Millimeter Wave Frequencies Using Meta-Heuristic Algorithms”. In: *Electronics* 8.11 (2019). ISSN: 2079-9292. DOI: 10.3390/electronics8111318. URL: https://www.mdpi.com/2079-9292/8/11/1318.

[42] M. Dong, T. Kim, J. Wu, and E. W.-M. Wong. “Millimeter-Wave Base Station Deployment Using the Scenario Sampling Approach”. In: *IEEE Transactions on Vehicular Technology* 69.11 (2020), pp. 14013–14018. DOI: 10.1109/TVT.2020.3026216.

[43] Q. Zeng. “Optimization of Millimeter-Wave Base Station Deployment in 5G Networks”. In: *2022 Thirteenth International Conference on Ubiquitous and Future Networks (ICUFN)*. 2022, pp. 117–121. DOI: 10.1109/ICUFN55119.2022.9829587.

[44] H. Miao and L. Xiong. “Channel Characteristics of Subway Station Based on Ray-Tracing at 5G mmWave Band”. In: *2020 IEEE/CIC International Conference on Communications in China (ICCC)*. 2020, pp. 687–692. DOI: 10.1109/ICCC49849.2020.9238885.

[45] P. Tang. “Channel Characteristics for 5G in Urban Rail Station at 3.5 GHz Based on Ray-Tracing”. In: *2021 7th International Conference on Computer and Communications (ICCC)*. 2021, pp. 2264–2268. DOI: 10.1109/ICCC54389.2021.9674363.

[46] M. Cudak, A. Ghosh, A. Ghosh, and J. Andrews. “Integrated Access and Backhaul: A Key Enabler for 5G Millimeter-Wave Deployments”. In: *IEEE Communications Magazine* 59.4 (2021), pp. 88–94. DOI: 10.1109/MCOM.001.2000690.

[47] C. Bektas, S. Böcker, B. Sliwa, and C. Wietfeld. “Rapid Network Planning of Temporary Private 5G Networks with Unsupervised Machine Learning”. In: *2021 IEEE 94th Vehicular Technology Conference (VTC2021-Fall)*. 2021, pp. 01–06. DOI: 10.1109/VTC2021-Fall52928.2021.9625210.

[48] Z. Zouhdi, B. Ratni, and S. N. Burokur. “Electronic Beam-Scanning Antenna Based on a Reconfigurable Phase-Modulated Metasurface”. In: *Sensors* 22.13 (2022). ISSN: 1424-8220. DOI: 10.3390/s22134990. URL: https://www.mdpi.com/1424-8220/22/13/4990.

[49] L. G. da Silva, P. Xiao, and A. C. S. “A 2-bit Tunable Unit Cell for 6G Reconfigurable Intelligent Surface Application”. In: *2022 16th European Conference on Antennas and Propagation (EuCAP)*. 2022, pp. 1–5. DOI: 10.23919/EuCAP53622.2022.9769482.

[50] O. Yurduseven, S. D. Assimonis, and M. Matthaiou. “Intelligent Reflecting Surfaces With Spatial Modulation: An Electromagnetic Perspective”. In: *IEEE Open Journal of the Communications Society* 1 (2020), pp. 1256–1266. DOI: 10.1109/OJCOMS.2020.3017237.

[51] L. Veluchamy, G. N. A. Mohammed, T. S. Krishnasamy, and R. Jyoti. “A wideband, single layer reflectarray antenna with cross loop and square ring slot loaded patch elements”. In: *International Journal of Microwave and Wireless Technologies* 11.7 (2019), pp. 703–710. DOI: 10.1017/S1759078719000187.

[52] E. Martinez-de-Rioja, Á. F. Vaquero, M. Arrebola, E. Carrasco, J. A. Encinar, and M. Achour. “Passive intelligent reflecting surfaces based on reflectarray panels to enhance 5G millimeter-wave coverage”. In: *International Journal of Microwave and Wireless Technologies* 15.1 (2023), pp. 3–14. DOI: 10.1017/S1759078722000721.

[53] M. H. Khoshafa, T. M. N. Ngatched, and M. H. Ahmed. “Reconfigurable Intelligent Surfaces-Aided Physical Layer Security Enhancement in D2D Underlay Communications”. In: *IEEE Communications Letters* 25.5 (2021), pp. 1443–1447. DOI: 10.1109/LCOMM.2020.3046946.

[54] L. Lai, J. Hu, Y. Chen, H. Zheng, and N. Yang. “Directional Modulation-Enabled Secure Transmission with Intelligent Reflecting Surface”. In: *2020 IEEE 3rd International Conference on Information Communication and Signal Processing (ICICSP)*. 2020, pp. 450–453. DOI: 10.1109/ICICSP50920.2020.9232092.

[55] H. J. Liong, C. W. R. Chiong, L. Gopal, and F. H. Juwono. “Sum-Rate Maximization for Intelligent Reflecting Surface Assisted MIMO SWIPT Systems”. In: *2022 IEEE Symposium on Future Telecommunication Technologies (SOFTT)*. 2022, pp. 47–51. DOI: 10.1109/SOFTT56880.2022.10009044.

[56] J. Lyu and R. Zhang. “Hybrid Active/Passive Wireless Network Aided by Intelligent Reflecting Surface: System Modeling and Performance Analysis”. In: *IEEE Transactions on Wireless Communications* 20.11 (2021), pp. 7196–7212. DOI: 10.1109/TWC.2021.3081447.

[57] Y. Xing, F. Vook, E. Visotsky, M. Cudak, and A. Ghosh. “Raytracing-Based System Performance of Intelligent Reflecting Surfaces at 28 GHz”. In: *ICC 2022 - IEEE International Conference on Communications*. 2022, pp. 498–503. DOI: 10.1109/ICC45855.2022.9838886.

[58] Z. Mohamed and S. Aïssa. “Leveraging UAVs with Intelligent Reflecting Surfaces for Energy-Efficient Communications with Cell-Edge Users”. In: *2020 IEEE International Conference on Communications Workshops (ICC Workshops)*. 2020, pp. 1–6. DOI: 10.1109/ICCWorkshops49005.2020.9145273.

[59] E. Björnson, Ö. Özdogan, and E. G. Larsson. “Intelligent Reflecting Surface Versus Decode-and-Forward: How Large Surfaces are Needed to Beat Relaying?” In: *IEEE Wireless Communications Letters* 9.2 (2020), pp. 244–248. DOI: 10.1109/LWC.2019.2950624.

[60] C. Huang, A. Zappone, G. C. Alexandropoulos, M. Debbah, and C. Yuen. “Reconfigurable Intelligent Surfaces for Energy Efficiency in Wireless Communication”. In: *IEEE Transactions on Wireless Communications* 18.8 (2019), pp. 4157–4170. DOI: 10.1109/TWC.2019.2922609.

[61] Q. Wu and R. Zhang. “Intelligent Reflecting Surface Enhanced Wireless Network via Joint Active and Passive Beamforming”. In: *IEEE Transactions on Wireless Communications* 18.11 (2019), pp. 5394–5409. DOI: 10.1109/TWC.2019.2936025.

[62] B. Zheng, C. You, and R. Zhang. “Double-IRS Assisted Multi-User MIMO: Cooperative Passive Beamforming Design”. In: *IEEE Transactions on Wireless Communications* 20.7 (2021), pp. 4513–4526. DOI: 10.1109/TWC.2021.3059945.

[63] Y. Han, S. Zhang, L. Duan, and R. Zhang. “Cooperative Double-IRS Aided Communication: Beamforming Design and Power Scaling”. In: *IEEE Wireless Communications Letters* 9.8 (2020), pp. 1206–1210. DOI: 10.1109/LWC.2020.2986290.

[64] J. Lyu and R. Zhang. “Spatial Throughput Characterization for Intelligent Reflecting Surface Aided Multiuser System”. In: *IEEE Wireless Communications Letters* 9.6 (2020), pp. 834–838. DOI: 10.1109/LWC.2020.2972527.

[65] M. A. Kishk and M.-S. Alouini. “Exploiting Randomly Located Blockages for Large-Scale Deployment of Intelligent Surfaces”. In: *IEEE Journal on Selected Areas in Communications* 39.4 (2021), pp. 1043–1056. DOI: 10.1109/JSAC.2020.3018808.

[66] C. Liaskos, A. Tsioliaridou, S. Nie, A. Pitsillides, S. Ioannidis, and I. Akyildiz. “An Interpretable Neural Network for Configuring Programmable Wireless Environments”. In: *2019 IEEE 20th International Workshop on Signal Processing Advances in Wireless Communications (SPAWC)*. 2019, pp. 1–5. DOI: 10.1109/SPAWC.2019.8815428.

[67] B. Sihlbom, M. I. Poulakis, and M. D. Renzo. “Reconfigurable Intelligent Surfaces: Performance Assessment Through a System-Level Simulator”. In: *IEEE Wireless Communications* (2022), pp. 1–10. DOI: 10.1109/MWC.015.2100668.

[68] D. Dampahalage, K. B. Shashika Manosha, N. Rajatheva, and M. Latva-aho. “Intelligent Reflecting Surface Aided Vehicular Communications”. In: *2020 IEEE Globecom Workshops (GC Wkshps.* 2020, pp. 1–6. DOI: 10.1109/GCWkshps50303.2020.9367569.

[69] D. Ding, D. Wu, Y. Zeng, S. Jin, and R. Zhang. “Environment-Aware Beam Selection for IRS-Aided Communication with Channel Knowledge Map”. In: *2021 IEEE Globecom Workshops (GC Wkshps)*. 2021, pp. 1–6. DOI: 10.1109/GCWkshps52748.2021.9681979.

[70] H. Choi and J. Choi. “WiThRay: Versatile 3D Simulator for Intelligent Reflecting Surface-aided MmWave Systems”. In: *2021 International Symposium on Antennas and Propagation (ISAP)*. 2021, pp. 1–2. DOI: 10.23919/ISAP47258.2021.9614590.

[71] URL: https://www.openstreetmap.org/.

[72] URL: https://maps.google.com/.

[73] Y. Zhang, D. J. Love, N. Michelusi, J. V. Krogmeier, S. Jyoti, A. Sprintson, and C. R. Anderson. “Improving millimeter-wave channel models for suburban environments with site-specific geometric features”. In: *2018 International Applied Computational Electromagnetics Society Symposium (ACES)*. 2018, pp. 1–2. DOI: 10.23919/ROPACES.2018.8364140.

[74] *Analysis of 28GHz and 60GHz Channel Measurements in an Indoor Environment*. URL: chrome-extension://efaidnbmnnnibpcajpcglclefindmkaj/https://telecominfraproject.com/wp-content/uploads/TIP_mmWave-Networks_Analysis-of-28GHz-and-60GHz-Channel-Measurements-in-an-Indoor-Environment_August-2019.pdf.

[75] H. M. Rahim, C. Y. Leow, T. A. Rahman, A. Arsad, and M. A. Malek. “Foliage attenuation measurement at millimeter wave frequencies in tropical vegetation”. In: *2017 IEEE 13th Malaysia International Conference on Communications (MICC)*. 2017, pp. 241–246. DOI: 10.1109/MICC.2017.8311766.

[76] *FACULTEIT TECHNISCHE NATUURKUNDE EN ELECTRICAL ENGINEERING, FLUX, TU EINDHOVEN*. URL: https://www.ahh.nl/index.php/nl/projecten2/9-onderwijs/20-faculteit-technische-natuurkunde-en-electrical-engineering-flux-tu-eindhoven.

[77] J. Mashino, K. Satoh, S. Suyama, Y. Inoue, and Y. Okumura. “5G Experimental Trial of 28 GHz Band Super Wideband Transmission Using Beam Tracking in Super High Mobility Environment”. In: *2017 IEEE 85th Vehicular Technology Conference (VTC Spring)*. 2017, pp. 1–5. DOI: 10.1109/VTCSpring.2017.8108644.

[78] URL: https://www.gsma.com/spectrum/wp-content/uploads/2019/10/26-and-28-GHz-for-5G-SPA.pdf.

[79] K. Qian, L. Yao, X. Zhang, and T. N. Ng. “MilliMirror: 3D Printed Reflecting Surface for Millimeter-Wave Coverage Expansion”. In: *Proceedings of the 28th Annual International Conference on Mobile Computing And Networking*. MobiCom ’22. Sydney, NSW, Australia: Association for Computing Machinery, 2022, pp. 15–28. ISBN: 9781450391818. DOI: 10.1145/3495243.3517024. URL: https://doi-org.tudelft.idm.oclc.org/10.1145/3495243.3517024.

[80] C. Levis, J. T. Johnson, and F. L. Teixeira. *Radiowave propagation: physics and applications*. John Wiley & Sons, 2010.

[81] A. Benoni, M. Salucci, G. Oliveri, P. Rocca, B. Li, and A. Massa. “Planning of EM Skins for Improved Quality-of-Service in Urban Areas”. In: *IEEE Transactions on Antennas and Propagation* 70.10 (2022), pp. 8849–8862. DOI: 10.1109/TAP.2022.3177284.

[82] M. D. Renzo, M. Debbah, D.-T. Phan-Huy, A. Zappone, M.-S. Alouini, C. Yuen, V. Sciancalepore, G. C. Alexandropoulos, J. Hoydis, H. Gacanin, and et al. “Smart Radio Environments empowered by reconfigurable AI meta-surfaces: An idea whose time has come”. In: *EURASIP Journal on Wireless Communications and Networking* 2019.1 (2019). DOI: 10.1186/s13638-019-1438-9.

[83] J. G. Andrews, X. Zhang, G. D. Durgin, and A. K. Gupta. “Are we approaching the fundamental limits of wireless network densification?” In: *IEEE Communications Magazine* 54.10 (2016), pp. 184–190. DOI: 10.1109/MCOM.2016.7588290.